An attempt at estimating Paris area CO_2 emissions from atmospheric concentration measurements

F.M. Bréon[1], G. Broquet[1], V. Puygrenier[1], F. Chevallier[1], I. Xueref-Remy[1], M. Ramonet[1], E. Dieudonné[1], M. Lopez[1], M. Schmidt[1], O. Perrussel[2], P. Ciais[1]

[1]: {Laboratoire des Sciences du Climat et de l'Environnement, UMR CEA-CNRS-UVSQ, Gif sur Yvette, France}

[2]: {AirParif, 7 rue Crillon, Paris, France}

Correspondance to : F.M. Bréon, (breon@lsce.ipsl.fr)

Abstract

Atmospheric concentration measurements are used to adjust the daily to monthly budget of fossil fuel CO_2 emissions of the Paris urban area, using as a first guess a spatially explicit emission inventory established by the Airparif local air quality agency.. We use 5 atmospheric monitoring sites including one at the top of the Eiffel tower. The atmospheric inversion is based on a Bayesian approach, and relies on an atmospheric transport model with a spatial resolution of 2 km with boundary conditions from a global coarse grid transport model. The inversion adjusts the CO_2 fluxes (anthropogenic and biogenic) with a temporal resolution of 6 hours, assuming temporal correlation of emissions uncertainties within the daily cycle, and from day to day, while keeping the a priori spatial distribution from the emission inventory.

The inversion significantly improves the agreement between measured and modelled concentrations. However, the residual misfits between the measurements and the model are often large compared to the measured CO_2 gradients between the sites that are used to estimate the fluxes, in particular at the Eiffel tower station. In addition, we sometime observe large model-measurement differences at stations upwind from the Paris urban area, which suggests a large and poorly constrained contribution from distant sources and sinks to the CO_2 concentration variability.

These results suggest that (i) the Eiffel tower measurements at 300 m above ground cannot be used with the current inversion system and (ii) the inversion should use the measured upwind-downwind gradients rather than the individual mole fraction measurements. With such setup, realistic emissions are retrieved for two 30-day periods. Similar inversions over longer periods are necessary for a proper evaluation of the optimized CO2 emissions against independent data.

1. Introduction

Although the total CO_2 emissions of developed countries may be well constrained from the total consumption of fossil fuel, its spatial and temporal distribution are not known with the same level of accuracy. In so-called bottom-up emission estimates, CO_2 emission is calculated as a combination of geo-referenced activity proxies (e.g. road traffic data, or number and type of buildings that relate to residential emissions, (Gurney et al., 2012)) multiplied by emission factors, accounting for the disaggregation of national annual budgets when dealing with regional or city inventories. The accuracy of the bottom-up inventories is seldom assessed and mostly relies on the difference between various estimates and on expert knowledge.

Due to the high population density associated with ground transportation, residence and industry, anthropogenic CO_2 emissions are large within cities (Pataki et al., 2006). The emitted CO_2 is transported in the atmosphere and results in elevated CO_2 concentration above and downwind of cities. There is therefore a potential to estimate the net CO_2 flux of a city from a few atmospheric concentration measurements located within or in the vicinity of the city (McKain et al., 2012). Over a very dense urban area, the net CO_2 flux is dominated by fossil fuel emissions, but over less dense urban structures, the net ecosystem exchange (NEE) becomes significant and can partly offset fossil CO_2 emissions during the growing season (Nordbo et al., 2012). Top-down net CO_2 flux estimates, constrained by independent atmospheric measurements, could come in complement to, or for the assessment of, current estimates that rely on bottom-up inventories.

The technique of estimating surface CO_2 fluxes from atmospheric composition measurements -and potentially from prior information- is relatively mature. It has been used for many years to estimate the biogenic fluxes at the global (Gurney et al., 2002;Chevallier et al., 2010), continental (Broquet et al., 2013;Peylin et al., 2005) and regional (Lauvaux et al.,

2009;Lauvaux et al., 2012) scales. However, because of uncertainties in the atmospheric transport, insufficient measurement sampling, and inconsistencies between the mathematical framework hypothesis of most inversions (e.g. no biases, Gaussian distribution of errors, uncorrelated observation errors) and the reality, the results are not always consistent, in particular at the regional scale, as shown for instance through the recent comparison of global and continental-scale biogenic flux estimates by several global inversons (Peylin et al., 2013).

Although the mathematical and modelling tools are similar, estimating the net CO_2 flux of a city amplifies the difficulties inherent to the atmospheric inversion. The spatial heterogeneity of the source and the possibility of having very high emission fluxes locally (e.g. a power plant) make the prior error statistics non Gaussian and the concentration plume highly variable. Relating mole fractions to city sources further requires accurate atmospheric transport model at fine scale. Atmospheric transport in urban areas is influenced by specific meteorological processes such as higher roughness of urban canopies (Zhao et al. 2014) and and urban heat island effects (Nehrkorn et al., 2013). For instance, (Pal et al., 2012) reported significantly thicker boundary layer over the Paris city than in the surrounding rural area during a four day campaign that took place in March 2011, which was interpreted as a consequence of the urban heat island effect. Another difficulty, shared with the inversion of biogenic fluxes, lays in the temporal variability of the fossil fuel emissions, which have a strong daily cycle but also day-to-day variability resulting from, for instance, temperature changes (through heating) or activity (e.g. traffic) variability. Last, measurements in and around a target city collect CO_2 molecules of various origins that must be separated into city sources and remote sources and sinks through the inversion.

This challenge has been addressed recently by several research projects, e.g. INFLUX (sites.psu.edu/influx, (Shepson et al., 2011)) over Indianapolis city or Megacities (http://megacities.jpl.nasa.gov; (Duren and Miller, 2012)) over Los Angeles, which have set-up a network of surface, tower and airborne measurements of the atmospheric CO_2 mole fractions. Satellite data may also provide valuable information as shown by (Kort et al., 2012). The results from the on-going urban CO_2 measurement project at Salt Lake City indicated that monthly emission relative changes of 15% could be detected at the 95% confidence level with the current monitoring system despite the inability to derive absolute estimates for a given month (McKain et al., 2012).

The CO_2-MegaParis project has a similar objective for the Paris area. This is a potentially favourable case as the city is very dense and the emissions intense over a limited surface, with a fairly flat topography in the surroundings, which makes the atmospheric transport modelling easier. A pilot campaign early 2010 was conducted in the framework of the MEGAPOLI project. Measurements of the mole fraction of CO_2 and its isotopes have been used to estimate the relative contribution of fossil and biogenic emissions in the concentration gradients (Lopez et al., 2013). The main campaign started in August 2010 with the installation of three CO_2 and CO monitoring stations within the city and its surrounding that provided near-continuous measurements until July 2011. These three stations complement two stations of the ICOS France network located in the Paris region outside the city that have been operational for several years. (Lac et al., 2013) made a first analysis of the measurements and a comparison against atmospheric modelling using the Meso-NH mesoscale transport model, combined with a surface scheme that accounts for the urban environment, for a period of 5 days in March 2011. They demonstrated the ability of the modelling framework to reproduce several features of the mixing layer height, as reported in (Pal et al., 2012), and of the mole fraction daily cycle.

Large efforts have been made by AirParif, the air quality agency for the Paris area, to generate an inventory of the Paris area emissions, for various pollutants and for CO_2 as well. The AirParif emission inventory, detailed in section 2.2, provides an hourly description of the CO_2 emissions at ≈1 km resolution for representative weekdays and months. We use this inventory as an input to the atmospheric transport simulations and compare the results to the atmospheric concentration measurements from the five sites. We then attempt a correction of the inventory based on the differences between the observed and modelled mole fractions. With only 5 stations in the vicinity of the city, there is likely not enough information to constrain the spatial distribution of the emissions. We therefore only rescale the emissions, relying on the spatial distribution provided by the Airparif inventory. For the inversion, NEE and fossil fuel emissions are optimized separately. We focus on two 30-day periods in the fall of 2010. This choice is driven by the expectation of rather small biogenic fluxes during this time period, which makes easier the interpretation of the measurements in terms of anthropogenic fluxes. Our objective is to assess whether a reliable estimate of the emissions can be derived from the combination of atmospheric measurements, available inventories and information on the atmospheric transport. A forthcoming paper will apply the methodology to a full year of observations and analyse the result for the spring and summer periods, when

CO_2 uptake by NEE can partially offset fossil fuel emissions (Pataki et al., 2007). In the following, section 2 analyses the time series of measured and modelled CO_2 mole fractions; section 3 describes the methodology to correct the inventory based on the measurement-model mismatches. The results are shown in section 4 and 5, using two different inversion setups. Section 6 discusses the results and concludes.

2. Measurements and direct simulations

2.1. CO_2 concentration measurements

In this paper, we use CO_2 mole fraction measurements that have been acquired continuously in the framework of the CO2-Megaparis and ICOS-France projects. Three stations have been equipped with high precision CO_2/CO analysers (Picarro G1302) specifically for the project objectives. One is located in the heart of Paris, at the summit of the Eiffel tower, 300 m above the surface. Two are located in the North and North-East of the Paris area in a mixed urban-rural environment. They are complemented by two ICOS-France stations that were operational before the start of the project. One is located in the South-West, about 20 km from the centre of Paris, while the other is a tall tower located further south by about 100 km. Both use gas chromatograph analysers (Agilent HP6890). The location of the stations are given in Table 1 and shown in Figure 1. They are very roughly located along a NE-SW direction, which defines the dominant wind directions, thus favourable for the estimate of the emissions from this observation network, with a station at the edge of the urban area in both directions. The measurements are quality-controlled and binned at a temporal resolution of 1 hour. They have been regularly calibrated against the WMO mole fraction scale (Zhao and Tans, 2006) so that measurement accuracy to the WMO-X2007 scale is estimated to be better than 0.38 ppm. The instrumental reproducibility is better than 0.17 ppm on the 5 minute average measurements available from the CO2-Megaparis stations, but the temporal averaging to the hourly-mean values used in this paper leads to precision much better than the accuracy (Zhao and Tans, 2006).

2.2. Atmospheric transport modelling

Atmospheric transport modelling provides the link between the surface fluxes and the atmospheric mole fractions. Here, we use the Chimere transport model (Menut et al., 2013) with a resolution of 2 km around the Paris city, and 10 km for the surrounding of the modelling domain (see Figure 1). There are 118x118 pixels in the modelling grid that covers an area of approximately 500x500 km^2. There are 19 layers on the vertical, from the surface

to 500 hPa. The Chimere transport model is driven by ECMWF-analysed meteorology at 15 km resolution. There is no urban scheme in the atmospheric modelling that is used here, which may be seen as a significant limitation to our inversion set-up. However, we conducted forward simulation comparisons between our modelling and that used in (Lac et al., 2013), which includes specific surface parameterization to account for the urban area, and we did not find significant differences on the simulated CO_2 mole fractions.

The model simulates the mole fractions that are driven by the surface fluxes and the boundary conditions. The surface fluxes that are accounted for in the simulations are the sum of

- Anthropogenic fossil fuel CO_2 emissions within the Île-de-France region, from the AirParif inventory, as described in section 2.3 and shown in Figure 2. Île-de-France is the administrative region spreading typically within 60 km around the Paris city, the boundaries of which are shown in Figure 1.
- Anthropogenic fossil fuel CO_2 emissions outside the Île-de-France region, according to the Edgar database [Edgar, 2011] available at 10 km resolution. These are only annual mean fluxes, and there is no diurnal or seasonal cycle.
- Biogenic fluxes from the C-TESSEL land surface model, as described in section 2.4.

The CO_2 boundary conditions prescribed at the edges of the simulation domain, and transported inside the domain by Chimere, are obtained from the Monitoring Atmospheric Composition and Climate (MACC) global inversion, v10.2) (http://www.copernicus-atmosphere.eu/). In this simulation, the global distribution of surface CO_2 fluxes has been optimized to fit the mole fractions measured at a number of stations distributed over the world, given their assigned uncertainty and prior information of the surface fluxes. Given the relatively coarse spatial resolution of the transport model used in the MACC inversion, CO_2 boundary conditions here are temporally and spatially very smooth and have little impact on the spatial gradients simulated within the domain area.

2.3. AirParif Inventory

The AirParif air quality agency (http://www.airparif.asso.fr/en/index/index) has developed an inventory of emissions (for greenhouse gases such as CO_2 but also for air pollutants) at 1 km spatial resolution and hourly time step for the Île-de-France region. The emissions are quantified by activity sectors. The improvement of methodologies and emission factors lead to frequent updates of the emission estimates.

Nearly eighty different source types are included in the inventory with three main classes: point sources, linear and diffuse sources. Point sources correspond to large industries, power plants, and waste burning; linear sources are related to transportation, while diffuse sources are mostly associated to the residential and commercial sectors. The road traffic emission estimates use a traffic model and vehicles counting devices that report the number of vehicles and their average speed over almost 40 000 km portions of roadways. Large industries are requested to report their CO_2 emissions and these are used in the inventory. For smaller industrial sources that are not required to report their emissions, a disaggregation of the regional fuel consumption is made based on the number of employees, leading to larger uncertainties. We have used the latest available version of the inventory, corresponding to year 2008, which has been developed for 5 typical months (January, April, July, August, and October) and three typical days (weekday, Saturday and Sunday) to account for the seasonal and weekly cycle of the emissions. Therefore this inventory estimates typical emissions but does not attempt to reproduce the daily variations resulting from specific meteorological conditions, or specific events such as public holidays.

Figure 2 shows an example of the spatial distribution of the total emissions for a weekday in October. Typical values are a few hundred $gCO_2\ m^{-2}\ day^{-1}$ within the city and a few tens $gCO_2\ m^{-2}\ day^{-1}$ in the suburbs. The main roads are clearly shown with flux enhancements of a few tens $gCO_2\ m^{-2}\ day^{-1}$, at the 1 km^2 resolution of the inventory. Further processing of this map shows that one third of the Île-de-France emissions are within 10 km of the Paris centre, and 61% are within 20 km.

There is a large temporal variation of emissions, as shown in Figure 3, mostly at the daily scale, but also at the weekly and seasonal scales. Most components show a large daily cycle with minimum emissions at night. During the day, the traffic related emissions show several maxima, in the morning, midday, and late afternoon. The daily cycles of the other activities are less pronounced but nevertheless significant. Point sources have the smallest daily cycle amplitude due to the industrial temporal profile that is relatively flat. The Paris area has few point sources and they contribute to typically 20% of the total emissions. The seasonal cycle is most pronounced for the residential emissions related to heating and cooking. One notes that residential CO_2 emissions do not go to zero during the summer months, because energy is still consumed for cooking and for heating water in summer.

In the following, the AirParif inventory for year 2008 is used as a prior estimate of the fossil fuel emissions within the Île-de-France region, both for the direct transport simulations (section 2.5) and for the flux inversion (section 3). Note that the inventory of point source emissions provides injection heights that have been used in the source term of the simulations. The AirParif inventory is provided as a function of legal time, and we have accounted for the time shift between legal time and UTC time, including the impact of daylight saving. Note that, due to the longitude of Paris, UT time and solar times are very similar.

2.4. Biogenic Fluxes

The Net Ecosystem Exchange fluxes used here are provided by the land surface component of the ECMWF forecasting system, C-TESSEL (Boussetta et al., 2013). They are extracted from the ECMWF operational archives at the highest available resolution, 15 km and 3 hours. These data are interpolated in space (2 to 10 km) and time (1 hour) to be consistent with our atmospheric transport model grid and temporal resolution.

Figure 4 shows the mean daily cycle of NEE for the Île-de-France area and for the 12 calendar months. There are large diurnal and seasonal NEE cycles. The flux is positive (emission) during the night and negative (uptake) during the day, even during the winter months, given the rather mild winter temperature prevailing over the Paris area. Nevertheless, the amplitude of the daily cycle of NEE is much larger in summer than it is in winter. The NEE values are of similar magnitude than the anthropogenic emissions with a strong anti-correlation on the daily cycle (negative NEE vs. large anthropogenic emissions during daytime; positive NEE and smaller anthropogenic emissions during the night). During the winter, NEE is relatively small and the anthropogenic emissions clearly dominate, but daytime NEE still offsets on average ~20% of the emissions, according to the C-TESSEL model simulations. During spring and summer, however, the daytime NEE uptake is larger in absolute value than the anthropogenic emissions as shown through a comparison of Figures 3 and 4.

The comparison of biogenic and anthropogenic fluxes over the Île-de-France area shows that they are of similar magnitude during spring and summer. The limited number of stations installed during the CO2-MEGAPARIS campaign is likely insufficient to properly distinguish their respective contributions, and there are significant uncertainties on the biogenic fluxes. As our main interest is the anthropogenic emissions, we chose to analyse a period when the biogenic flux is small, i.e. during fall and winter. The present paper focuses on two 30-day periods that start on October 21st and November 27th 2010. During these periods, the monthly

mean hourly NEE fluxes are less than 3 ktCO_2 per hour over the Île-de-France area. NEE is then small, but not negligible, compared to anthropogenic emissions during the chosen inversion period.

2.5. Direct CO_2 transport simulations

Figure 5, together with Figure S-1 in the supplementary, shows the time series of the CO_2 mole fractions together with an indication of the modelled wind speed and direction to help the interpretation of the results. These time series are derived from observations and direct atmospheric modelling as described in section 2.2.

The Trainou (TRN) station (bottom row) is far from the Paris agglomeration. In addition, the measurement inlet is at 180 m from the surface. It shows a diurnal cycle amplitude that is much smaller than at the other sites. In addition, the modelled contribution from both anthropogenic and biogenic fluxes within the simulation domains is limited to a few ppm, as shown by the difference between the black and green curve. There are a few exceptions however, essentially when the wind blows from the North, i.e. from the Paris city, and transports CO_2 to the TRN rural site. The best examples are around Dec 8th and Dec 23rd. For these particular cases, the measurements at TRN are significantly larger than the model results. The underestimate by the model is not limited to these dates and there are significant discrepancies between the model and the measurements at this background site, in particular at the end of November and at the beginning of December.

The other sites are much closer to Paris and are then more affected by the fossil CO_2 emissions. At Gif-sur-Yvette (GIF) the largest mole fractions are observed when the wind is from the North-East, which is expected as the Paris city is in that direction. There is also an impact of the wind, as the largest mole fractions are measured in low wind speed conditions. During the Oct-Nov period (Figure S-1), the wind is mostly from the South and South-West, thus not from the city, and there is a relatively good agreement between the modelled and measured mole fractions. In December, the wind direction is more variable, the fossil CO_2 signal appears much larger, and there are very significant differences between the measurements and the model estimates.

Gonesse (GON) is located to the North of the city, while Montgé-en-Goële (MON) is further away to the North-East. The shorter distance to the main source may explain the larger signal at the former station. The only cases when the modelled anthropogenic contribution is small at GON (small difference between black and green curve) is when the wind is from the North.

For other wind directions, the modelled signal is strong -more than 10 ppm- and there are large differences between the measurements and the modelling results. During December, the measurements are most often larger than the model estimates. A similar observation can be made at MON. Surprisingly, the measurements are significantly larger than the modelling results, even when the wind blows from the North or North-East, i.e. when the Paris agglomeration contribution is negligible (Dec 3rd, Dec 6-9, Dec 22-23). For these cases, the most likely explanation is an underestimate of modelled CO_2 from the boundary conditions or from emissions within the modelling domain outside of Île-de-France. Hereafter, we shall denote this contribution as that from "remote fluxes". Note that this impact from remote fluxes shows a large increase of the mole fraction for the periods discussed above. We may then hypothesize that this increase is underestimated. The interpretation is that anthropogenic emissions from the Benelux area generate high concentrations that are underestimated in the boundary condition field that is used in our simulations.

The EIF site is at the top of the Eiffel tower, 300 m above the Paris city. The wind speed for this station is larger than for the other one, simply because it is higher in altitude. One expects atmospheric mixing between the surface emissions and the inlet, so that the measurements are representative of a larger area than e.g. MON and GON. Nevertheless there are some very significant differences between the modelled and the observed mole fractions at EIF. The differences may be huge, larger than 30 ppm, even during the afternoon, e.g on Oct 24th, Nov 7th, Dec 3rd, Dec 12th. Clearly, our atmospheric modelling framework cannot properly represent the mole fraction time series at the EIF station, either because of strong local (sub grid cell) emissions, or because of atmospheric transport processes that are not properly represented, in particular concerning the vertical transport above the city. Further analysis of the model-measurement mismatch is shown in Figure S- 2. The largest mismatches are preferentially observed during the morning and for low wind speeds, but are observed at all hours of the day and for all wind speed and directions. A forthcoming paper will present an in-depth analysis of the CO_2 mole fraction variability at each station.

The curves in Figure 5 and Figure S-1 show very large temporal variations of CO_2 within a day at all stations. Further analysis confirms that the largest variations are observed during the night, when the mixing layer is shallow. During the night and morning, the atmosphere is often very stable so that surface emissions accumulate within the lowest atmospheric layers, the thickness of which ranges from a few meters to tens of meters. The atmospheric mole

fraction is then mostly sensitive to local fluxes and vertical mixing -an atmospheric process that is difficult to model- so that there is a large uncertainty about the link between the emissions and the atmospheric mole fraction. It is then clear that the night-time and morning measurements are not appropriate for our flux inversion, as inverting them would be too sensitive to atmospheric transport biases. As a consequence, we focus on the concentration measurements acquired during the afternoon only, from noon to 4 p.m., when the mixing layer is usually well developed. This justifies our choice of selecting only hourly measurements between noon and 4 p.m.. The daily averages of these afternoon measured and modelled values are shown in Figure 5 as diamond symbols.

2.6. Analyses and insight for the inverse modelling configuration

Both the measurements and the modelling results show a large impact of the Paris area anthropogenic emissions on the CO_2 mole fractions at the 5 sites analysed here. The mole fraction increases over the modelled large-scale value depends on the wind speed and direction and a typical order of magnitude is 10 ppm. As expected, the signal is smaller for the rural station of TRN, which is further away from the city than the other sites. Many of the features in the measured time series are well reproduced by the modelling framework, which gives some confidence in its usefulness to improve the emission estimates.

There are also some significant differences between the measured and modelled mole fractions that cannot be justified by inaccurate emission inventories. The most obvious such feature is the mole fraction underestimate in northerly wind conditions when the MON and GON sites are little sensitive to the Île-de-France emissions. This feature strongly suggests that remote fluxes lead to mole fraction increases that have biases with a typical magnitude that is similar to the impact of the Paris area emissions. These biases may have a significant impact on the flux inversion results. On the other hand, as the impact from remote fluxes is large scale, one may expect that this impact is similar for monitoring stations upwind and downwind from the Paris urban area. The boundary condition error may then be strongly reduced when analysing the difference between two stations mole fractions. On the other hand, the mole fraction difference between two stations may contain information on the Île-de-France emission when one lies upwind and the other downwind from the city. It then suggests the use of downwind-upwind gradients in the CO_2 mole fractions rather than the absolute value of CO_2 measurements in the inversion procedure.

The other significant feature in the comparison of the modelled and measured CO_2 mole fractions is much larger errors at the EIF site than at the other stations. Clearly, the modelling of the atmospheric transport is inaccurate for this particular site. We put significant efforts to understand the origin of the large model-measurements mismatches at EIF (see supplementary Figure S- 2). Large modelling errors are observed for all wind directions. These results illustrate the difficulty in modelling the CO_2 mole fraction within cities, even with a measurement inlet in altitude, well above the sources. Note that (McKain et al., 2012) also find very large (>30 ppm) model-measurement mismatches within the urban area of Salt Lake City, even when using a high-resolution model. Similarly (Lac et al., 2013) finds large model-measurements differences at EIF despite the use of a urban parameterization in the modelling. The inability to properly model the CO_2 signal at EIF may have detrimental impact on the emission estimates derived from atmospheric inversion. Conversely, the forward simulations show that the TRN site is little sensitive to the Paris area emissions due to its location further away from the city than the other sites. Consequently, it cannot be used as a "downwind" site; in addition, GIF is better suited as an "upwind site" for southerly conditions as it is closer to the urban area and provides therefore a better information on the air composition as it enters the city. These features suggest not to use EIF and TRN and rather focus on MON, GON and GIF to estimate the Paris area emission from their measured mole fractions.

The main objective of the "gradient" inversion method is thus to focus on the monitoring stations that are in the close vicinity of the urban area and to estimate the city scale emissions by removing most of the upwind signal from the measured and modelled concentrations. The upwind signal is driven by remote fluxes both from the boundary conditions and by fluxes within the domain but outside the city that are poorly modelled. The inversion method also attempts to select the downwind measurements that are strongly affected by the city emissions, in an attempt to minimize the impact of aggregation errors. Ideally, we would select only the wind direction when one station lies directly downwind from another, with the Paris city in between. However, given the very limited network of stations surrounding Paris, we have to broaden significantly the range of acceptable wind directions.

In the following, we therefore describe two attempts at inverting the Paris area emissions from the concentrations. The first one uses the 5 site records and relies on the boundary conditions provided by the large scale model. The second one only uses the measurements

from GON, MON and GIF that are near-surface stations in the near vicinity of the Paris city, and the flux inversion is based on the CO_2 mole fraction gradients between the upwind and downwind stations, a method which requires the selection of favourable wind conditions. The mathematical framework is very similar for these two inversions and is described in the next section. The results for the inversion based on the 5 site measurements are discussed in section 4; those for the inversion based on the gradients are in section 5.

3. Flux inversion

3.1. Principles

We follow a linear Bayesian inversion approach with Gaussian error statistics to determine the optimal surface fluxes (anthropogenic emissions and biogenic fluxes) and their uncertainties from a prior estimate of the fluxes and their uncertainties and from the mole fraction measurements.

We call $\mathbf{x}$ the state vector that gathers the scaling factors for the 6-hourly flux maps, $\mathbf{x_B}$ its prior estimate, $\mathbf{H}$ the matrix operator that relates state parameters and mole fraction variations according to the atmospheric transport model, $\mathbf{y}$ the observed mole fractions or mole fractions gradients, $\mathbf{y_F}$ the simulated impact on these mole fractions of the lateral boundary conditions and of the fluxes that are not accounted for in the state vector, $\mathbf{B}$ the uncertainty covariance matrix of $\mathbf{x_B}$, and $\mathbf{R}$ the error covariance matrix of $\mathbf{y}$. These components are detailed in the next section.

The optimal solution is given by (Tarantola, 2005):

$$\mathbf{x_A}=\mathbf{x_B} + (\mathbf{B^{-1}} + \mathbf{H}^{\mathrm{T}}\,\mathbf{R}^{-1}\,\mathbf{H})^{-1}\,\mathbf{H}^{\mathrm{T}}\,\mathbf{R}^{-1}\,(\mathbf{y} - \mathbf{y_F} - \mathbf{H}\,\mathbf{x_B}) \quad (1)$$

and its posterior error covariance matrix is

$$\mathbf{A} = (\mathbf{B^{-1}} + \mathbf{H}^{\mathrm{T}}\,\mathbf{R}^{-1}\,\mathbf{H})^{-1} \quad (2)$$

Note that A does not depend on the actual measurement values, but varies, among other factors, with their temporal and spatial sampling.

3.2. State vector: x

Both the anthropogenic and biogenic prior fluxes described in Section 2 show a large diurnal cycle that impacts the model simulations of CO_2, and that is uncertain. It then appears useful to invert this cycle together with the flux mean value. However, as discussed earlier, only CO_2 measurements during the early afternoon can reliably be used to estimate the fluxes and their information from CO_2 measurements about the daily cycle is rather poor. We limit the

number of independent periods to 4 corresponding to the local times between 0-6 h, 6-12 h, 12-18 h, and 18-24 h, respectively.

For the fossil fluxes, we use independent scaling factors for each individual day in the state vector, which makes the number of corresponding variables amount to 30×4=120 for the 30-day period of the inversion. These scaling factors apply to the prior flux estimates derived from the AirParif inventory and are noted $\lambda^i_{0-6}, \lambda^i_{6-12}, \lambda^i_{12-18}, \lambda^i_{18-24}$ with i between 1 and 30.

Similarly, we optimize scaling factors of the prior NEE flux from C-TESSEL. The simulation domain shown in Figure 1 is split into 3×3 large boxes, and we choose the same 6-hour periods than for the anthropogenic fluxes to optimize scaling factors of NEE. However, we do not attempt a daily retrieval of NEE, and considered a single scaling factor for optimizing monthly NEE each 6-hour window over a 30-day inversion period. The number of variables to optimize NEE is therefore 3×3×4=36. In the following, these NEE scaling factors are shown as $\alpha^X_{0-6}, \lambda^X_{6-12}, \alpha^X_{12-18}, \alpha^X_{18-24}$ where X is one of the 9 large boxes. One of the 9 boxes covers the Île-de-France region, the other ones are in the surrounding. In the *Inversion results* sections, we analyse the inversion of NEE for the centre box (X=C) together with those for the anthropogenic emissions. The surrounding boxes provide some degree of freedom to the inversion system to adjust the likely biased boundary conditions.

Finally, there is one monthly variable (C_{Offset}) in the state vector to adjust a possible large scale offset on the modelled concentrations over the domain and 30-day period.

The state vector **x** for the linear inversion has therefore 120+36+1 = 157 variables. The prior estimate for C_{Offset} is 0 as the modelled is expected to reproduce the large-scale concentration with no bias, since CO_2 boundary conditions are from a global inversion making use of global station observations during the same period than the inversion 30-day periods. All other components of the state vector represent scaling factors to the modelled fluxes and have therefore a prior value of 1.

3.3. Measurements: y

y contains the measurements that are used to constrain the flux inversion. As explained above, we only use hourly measurements that have been acquired during the afternoon from noon to 4 p.m. local time. In addition, the measurements need to be representative of a relatively large area to reduce the sensitivity to local, unresolved, fluxes. This condition is not met when the wind speed is low. We therefore use for the inversion only the measurements

filtered for wind speeds larger than a given threshold. In the version of the inversion system used here, the threshold is set at 2 m s^{-1}. The wind speed is that analysed by the ECMWF at the location, height, and time of the observation. This criterion retains about 70% of the potential measurements. Note that the wind generally increases with altitude so that a larger fraction of observations are considered valid at the tower sites (TRN and EIF) than at the others.

In Equation (1) the mole fraction measurements **y** are corrected for the contributions that are not accounted for in the state vector ($\mathbf{y}_F$). $\mathbf{y}_F$ are the modelled mole fraction accounting for the boundary conditions and anthropogenic fluxes outside Île-de-France (prescribed from the Edgar database). This contribution is shown as a blue line in Figure 5 and Figure S-1.

One version of the inversion system uses the measured mole fractions at the 5 sites. Following the discussion of Section 2.6, the other version is based on the gradients between the stations in the borders of the city area, i.e. GIF, MON and GON: When the wind is from the South-West (upwind direction between 160° and 260°), GIF is considered as upwind from the city, and the corresponding **y** elements are the differences between the mole fractions measured at either MON or GON and that measured at GIF. Similarly, when the wind is from the North-East (upwind direction between 0 and 135°), MON is used as an upwind reference to the GIF or GON mole fraction measurements. For other wind directions, the measurements are not assimilated.

3.4. Prior flux uncertainties and error correlations: B

Although we invert the scaling factors of fossil CO_2 emissions for each day and each 6-hour period, the uncertainties in these factors are correlated. We therefore attempt to assign correlations for the prior uncertainties based on several considerations: (i) the monthly budget for the AirParif inventory is generally stated to have an uncertainty of 20% which is used here; (ii) we assume small positive correlations between the different 6-hour windows; (iii) we assume stronger correlations from day to day for a given 6-hour window; (iv) the a priori uncertainty of individual 6-hour emission should have a typical order of 50%.

Based on these considerations, we set, rather arbitrarily, prior error correlations to 0.4 for two adjacent time periods (e.g. 12-18 and 18-24) and to 0.2 for non-adjacent time period (e.g. 6-12 and 18-24). For successive days, we use an exponential de-correlation with a characteristic time T_{cor}. The correlation between the prior uncertainties of the fossil CO_2 emissions scaling factors is then the product of this exponential and the time correlation. For instance, the

correlation between λ_{0-6}^{5} and λ_{6-12}^{9} is $0.4\exp(-4/T_{cor})$. The results shown in this paper have been mostly obtained with a temporal correlation T_{cor} of 7 days, but other values, from 1 to 30 days, have been also tested. We have verified that such a **B** matrix is positive-definite. The desegregation of the assumed 20% uncertainty for the monthly emission totals, based on these temporal correlations, results in a standard deviation of uncertainties for individual 6-hour period of 33% (T_{cor}=30 days) to 50% (T_{cor}=7 days).

For the biogenic flux scaling factors, we set a relative prior uncertainty (standard deviation) close to 0.70 with some variations according to the box size (the variance varies inversely to the surface of the box), based on the numbers derived at 0.5° resolution in (Broquet et al., 2011). We do not assign any spatial / temporal correlation between the various biogenic scaling factors, i.e. between the 9 boxes or the 4 time periods. Similarly, there is no correlation in **B** between the prior uncertainties on the biogenic and anthropogenic fluxes, neither between the offset mole fraction and the other parameters in the state vector. For C_{offset}, we assign an uncertainty of 5 ppm, corresponding to typical large-scale variations of the mole fractions at the boundary conditions.

3.5. Operator matrix: H

The operator matrix **H** provides the link between the surface fluxes and the mole fraction measurements. It combines the spatio-temporal distributions of the fluxes, both for the AirParif inventory and the C-Tessel biogenic fluxes, that are assumed and not modified through the inversion, the atmospheric transport by the Chimere model, and the sampling of the atmosphere at the instrument locations. Note that the AirParif inventory has a 1 hour temporal resolution. The direct simulation (**H x**) uses the description of the emissions at this temporal resolution. Each element of the state vector, except for C_{Offset}, corresponds to a natural or anthropogenic surface flux for a larger time period. We use the atmospheric transport model to compute the impact to the mole fraction of each surface flux (156 in total) corresponding to an element of the control vector. The 4D mole fraction fields from each of these simulations are then sampled at the place and time of the atmospheric observations. This provides the elements of each column of the **H** matrix.

For the *gradients* version of the inversion, the sampling is set as the difference between the simulated mole fractions at the two sites that are considered when the wind direction conditions described in section 3.3 are verified. By definition of this parameter, the column

of the **H** matrix that corresponds to C_{Offset} is set to 0 for the gradient version of the inversion, and 1 ppm for the other version.

3.6. Observation error: R

The measurements provided by the instrument are precise, certainly better than 0.3 ppm. However, the observation error in **R** also includes any source of misfit between the model and the data that is not accounted for in the control vector such as the representation error, the impact of the error in the spatial distribution of the fluxes, and the atmospheric transport modelling error. These are difficult to assess (Broquet et al., 2013) although one expects significant values given the very heterogeneous urban environment that is discussed here.

Due to the complexity and misunderstanding of the processes underlying the observation error, that may lead to positive or negative correlations, we ignore observation error correlations in the construction of **R**, which is thus diagonal, both when assimilating individual mole fraction measurements and when assimilating mole fraction gradients.

We use two statistical diagnostics of the misfits in the observation space described by (Desroziers et al., 2005) to infer typical observation error variances: (i) the agreement between the sum of the uncertainty from the prior estimate of the control parameters and of the observation error with the RMS of the prior misfits to the assimilated data; and (ii) the agreement between the observation error with the mean of the product of prior and posterior misfits to the assimilated data. Based on this analysis, we infer a 10 ppm observation error for the EIF station and 5 ppm for the other sites when assimilating individual mole fraction measurements. When assimilating mole fraction gradients, we set a 3 ppm observation error.

We acknowledge that the two configurations are not consistent with each other. Indeed, if the observations errors were truly uncorrelated, as indicated by the use of a diagonal matrix for **R**, the errors on the mole fraction gradients should be larger, by a factor $\sqrt{2}$, than those of the individual observation. In practice, we set smaller errors for the gradient observations. The argument for the gradient inversion set-up is that the observation errors are strongly correlated between measurement sites at a given time due to the large scale impact of the remote fluxes. Thus, the inconsistency lies in the set-up of a diagonal R matrix when we know that there are positive correlations in the observation errors.

4. Results

We present below the results obtained with the first version of the inversion system that uses the mole fraction measurements at all five sites. Section 5 shows the results based on the concentration gradients between the 3 sites that are at the border of the Paris agglomeration.

4.1. Daily fossil fuel CO_2 emissions

Figure 6 shows the daily anthropogenic fluxes inferred by the inversion. Here, we have aggregated the 4 6-hour periods as well as their uncertainty, accounting for the error correlations between the periods. Although the inversion controls scaling factors, we show here the resulting fluxes expressed in $MtCO_2$ per day. There is a clear weekly cycle on the emissions that are smaller during the week-ends. One may also note a shift in emission between Oct 29th and Nov 1st that corresponds to a change of month and therefore the switch to a different dataset in the AirParif inventory. The Airparif inventory includes a profile for October. For November and December, Airparif recommends the use of the January emission profile. The theoretical posterior uncertainties are smaller by a factor of typically two than the prior values. The day-to-day variations of the posterior fluxes are, however, surprisingly large. The largest flux corrections can be easily traced back to measured mole fractions larger than the prior modelled values: at the beginning of the first period, mole fraction measurements are much larger than the prior simulation, in particular at GON and EIF. Note that winds are rather small during the first days, below the 2 m s^{-1} threshold, so that the MON and GON measurements have not been used for the inversion. Dec 3rd is another day with low wind speeds, but the MON observation meets the wind speed threshold and is much larger than the prior. The EIF measurement is also very large compared to the simulation. Similar conditions appear for Dec 21st and only the EIF measurements drive the inversion. These observations suggest that low wind speeds lead to unreliable inversion results in this configuration, likely because of unresolved local sources influencing the sites, even with the 2 m s^{-1} threshold that we use for selecting observations. At the other extreme, the inversion infers a very low flux for Dec 4th. This can be traced back to measurements that are smaller than the prior by about 10 ppm at all operating sites (GIF was down). There is nothing specific for the wind on this particular day while the large scale concentration (blue line) shows a local maximum that does not appear in any of the station site measurements. The contribution from remote fluxes then is most likely responsible for the misfit during that particular event.

We also tested similar inversions using different error correlation times (T_{cor}) in the range of the synoptic to seasonal time scales that drives the emission variability. With a 1 day error correlation time, rather than 7 days used in our standard configuration, there are days with little or no flux constrain by the observations, while there is no smoothing of the day-to-day variability, resulting in an even larger spread of the retrieved fluxes (not shown). The low estimate that is obtained on Nov 4th (Figure S- 3) becomes negative, which is unrealistic, and the largest daily values are close to 0.5 $MtCO_2\ day^{-1}$. At the other extreme, a 30-day correlation time leads to much smoother results (See Figure S- 4). Most of the daily-optimized flux estimates remain within the prior uncertainty range. The weekly cycle is apparent in the posterior fluxes but is driven by the prior rather than the observations.

4.2. Diurnal cycle

Figure 7 shows the monthly mean flux estimates for the Île-de-France region for the various 6-hour periods. It shows the results of the inversion for the anthropogenic emissions, the NEE, as well as the total. Note that the total estimate is necessarily the sum of the biogenic and anthropogenic fluxes. Conversely, the uncertainty range is not a simple sum as it accounts for the correlations between NEE and fossil CO_2 emission errors in the **A** matrix.

As expected, the flux inversion has very little impact on the optimized fluxes for the 0-6 and 18-24 periods. This is because we only use measurements between noon and 4 p.m., which are little affected by the emissions and sinks from these nocturnal time periods. On the other hand, the anthropogenic flux uncertainty is strongly reduced (by more than a factor of 3) for the 6-12 and 12-18 time periods, when measurements are assimilated. The anthropogenic flux estimate shows limited change from its prior estimate and it remains within the prior uncertainty. In this inversion set, the largest change from the prior estimate is for the NEE, for the period 12-18 h during the Nov-Dec period. One notes that the posterior estimate of the afternoon NEE is slightly positive from a strong negative value, and outside of the prior uncertainty range.

The uncertainties on the total flux are similar to what is expected for an uncorrelated sum of the biogenic and fossil CO_2 fluxes uncertainties, i.e. a quadratic sum. It is slightly smaller for the afternoon period due to a negative correlation (-0.35) between the posterior uncertainties of NEE and fossil CO_2 fluxes for both 30-day periods. Other periods show much smaller correlations. These numbers indicate that the observation sampling provides significant information to distinguish NEE from fossil CO_2 fluxes in the inversion. Although a given

measurement cannot trace the origin of the mole fraction excess, the assigned biogenic and anthropogenic flux errors have different spatial and temporal patterns which are exploited by the inversion system to attribute the mole fraction signal to specific sectors. However, this attribution relies on the a-priori spatial and temporal distribution of the fluxes that are affected by uncertainties. Thus, the theoretical ability of the system to disentangle natural and anthropogenic fluxes may not be realized in practice.

Of note is the peculiarity of NEE during the 6-12 h period of Oct-Nov (Figure S- 5). The NEE flux and uncertainty range are very close to zero. This corresponds to the total NEE of the 6 h period. The flux is generally positive, indicating emission, during the early hours, and negative, indicating a sink, later on within this 6 hours period. The inversion corrects the value of α^{C}_{6-12} (the posterior value is 1.36 for a prior value of 1) and therefore the amplitude of the NEE cycle. It has however little impact on the total flux during the entire 6 hour period, so that optimized NEE values remains much smaller than the anthropogenic flux or the biogenic fluxes during the other time periods.

4.3. Impact of the flux correction on the CO_2 mole fractions

Figure 8 and Figure S- 6 show scatter plots of measured versus modelled mole fractions. The first row of the plots on each of these figures shows the modelled mole fractions from the domain boundaries and the fossil CO_2 emission outside Île-de-France (blue lines in Figure 5, $\mathbf{y}_F$ in equation 1) against the measurement. This constitutes the modelled contribution to the mole fraction that is not optimized by the inversion. For the TRN tall tower site, that is far from Paris, there is a fairly good agreement between measured and modelled mole fractions during the first period (Oct-Nov, in supplementary). It is interesting to note that the second period (Nov-Dec) shows a much larger observed variability of CO_2 at TRN than the first one does. This variability is well reproduced by the model (correlation is 0.81) although the slope of the best linear relationship is clearly smaller than 1. Similarly, the GIF site shows a much larger variability during the second period than during the first. This is well explained by the fact that, during the first period, the wind is mostly from the South and the South-West so that GIF is not significantly affected by the Paris city emission. For other cases, there is a large spread in the scatter plots, which is expected as the Paris city emissions affect the measurements but not the modelled values that only account for the domain boundaries and the anthropogenic emissions outside Île-de-France.

The second row shows simulated CO_2 induced by prior NEE and fossil CO_2 fluxes (i.e. those that are optimized through the inversion) against measured mole fractions corrected for the large scale values (i.e. $\mathbf{y}_F$, shown on the Y-axis of the first row). Although there is a large spread, the correlation is significant, which shows that the transport model and the prior flux set up have altogether some ability to reproduce the observed CO_2 mole fraction variability. During the Oct-Nov period, the biases are fairly small at all sites except EIF; during the Nov-Dec period, the comparison show much larger negative biases up to -13 ppm at EIF and -9 ppm at MON. The standard deviation of the measurement-model difference varies with the sites and period, between 3.1 and 15.3 ppm. They are larger for the later period than for the earlier one and smaller at TRN than for the sites that are closer to Paris.

After the inversion, the agreement is significantly improved as shown in the third row, although there are sites where either the bias or the standard deviation of the model-data misfit is degraded. The change in bias between the prior and posterior values is mostly explained by the optimized offset mole fraction C_{Offset}. It is 1.8 ppm for the Oct-Nov period and 5.1 ppm for the Nov-Dec period. Thus, the inversion system corrects for the measurement biases by adjusting the large scale offset rather than the fossil CO_2 emissions or NEE fluxes in the model domain. For both periods, the biases at EIF, both prior and posterior, are much larger than for the other sites. Also, the hypothesis of a large-scale constant and uniform bias in the modelled mole fractions, underlying the use of C_{offset} within the inversion, is not compatible with the observations at TRN, a site that is mostly outside the Paris agglomeration influence. After the inversion, the bias of the modelled CO_2 mole fraction at TRN is larger than in the prior. Although the inversion interprets biases as resulting from a large-scale signal to be corrected by optimization of C_{offset}, this does not seem consistent with the measurements. The origin of the discrepancy lies in the very large biases at EIF. This confirms that the atmospheric transport modelling does not reproduce the mole fractions properly at the top of the Eiffel tower. Again, there seems to be specific features in the atmospheric vertical transport over the Paris city or local emissions beneath the EIF tower location that are not well represented in the model used in this study, and that lead to higher mole fractions at this location.

After the inversion, the standard deviation of the CO_2 modeled-measurement mismatch is between 3.7 and 5.2 ppm except for EIF where it reaches 13.4 ppm. The standard deviation is always significantly larger than the bias, so that the RMS error is similar to the standard

deviation. Again, the EIF site appears poorly represented compared to the other sites. We have therefore attempted an inversion excluding the measurements from that particular site. The inversion results appear only slightly more realistic: C_{Offset} is then 1.2 ppm and 4.5 ppm for the two 30-day periods, compared to 1.8 ppm and 5.1 when EIF is assimilated. The statistics at the various sites are also slightly improved, but the daily flux retrievals (as those shown in Figure 6) are still highly variable.

5. Results for the inversion based on the concentration gradients

We now present the inversion results where the input observation are the spatial gradients between two measurement sites with a reference site chosen upwind the urban area, as described in section 3.3. Figure 9 and Figure S-6 show the time series of these afternoon mean differences. The prior value is almost always positive, because the reference is chosen upwind the Paris agglomeration. There are a few exceptions, like on Dec 22nd at GON. On this particular date, the reference chosen is MON according to the wind direction. Further investigation demonstrated that this unexpected behaviour is linked to a large spatial gradient of the CO_2 concentration generated by anthropogenic emissions over the Benelux accounted for in the Edgar inventory and transported by the Chimere model ($\mathbf{y}_F$ in equation 1). Interestingly, the observations confirm the sign and the order of magnitude of the gradient that is modelled with our setup that uses crude anthropogenic emissions outside Île-de-France. The scatter plots of Figure 10 confirm that the modelling of gradients is much more consistent with observations than that of the absolute mole fractions (Figure 8). Indeed, the prior model-measurement correlations range from 0.47 and 0.82 for the latter, when they are from 0.83 to 0.93 for the former. These scatter plots strongly support the hypothesis that the modelling errors are spatially correlated and result, to a large extent, to erroneous constraints in the large-scale mole fraction patterns. It justifies the inversion set-up based on the concentration gradients that is discussed in this section.

Although the modelling expects positive upwind-downwind mole fraction gradients, the observed values can be negative both at GON and GIF. At GON, negative values are found only in Northerly wind conditions, i.e. when MON is used as a reference. As GON is in the northern part of the Paris agglomeration, one expects a smaller signal than for southerly wind conditions. The negative gradients values using GIF as a reference, in particular that of Dec 3rd are more surprisingly and we could not find a valid explanation for them.

As expected, the posterior estimates of the mole fractions gradients are closer to the observations than the prior. This is better shown in Figure 10, which confirms that the statistics of the mole fraction gradients have been significantly improved through the inversion. Note however that the standard deviation for the MON site (when GIF is used as a reference) is slightly degraded from the prior value of 2.0 ppm. After the inversion, the correlation between optimized and observed CO_2 gradients for all three stations is larger than 0.90. For the other time period shown in the supplementary material (Figure S- 8), the correlation statistics are not as good. However, this is due to a lower variability of the gradients, and the posterior standard deviations are 2.3, 2.7 and 2.3 ppm for the three sites, and are then similar as the values shown in Figure 10.

The inverted daily fluxes based upon the gradient inversion are shown in Figure 11. The uncertainty reduction is significant for all the days of the two time periods and a typical order of magnitude is a factor of 2, like in the inversion of absolute mole fractions at each site. The emission uncertainty is reduced even for days with no usable measurements, when the wind direction is not within any of the two ranges defined in section 3.3, due to the temporal correlation of the uncertainties and thus of the corrections applied to the prior (section 3.4). The deviations of the flux estimate from the prior follow the gradient observation deviation from the model (see Figure 9). These deviations are mostly negative, although they are positive for a few days during both time periods. For the Nov-Dec period, the posterior emission estimates are within the bounds of the prior uncertainty range. On the other hand, the posterior estimate is much lower than the prior flux during the second half of the Oct-Nov period (Figure 11, top). Interestingly this period (Nov 1st to Nov 20st, 2010) was very mild [Meteo France, 2010] which suggests that the heating sector emissions were well below the AirParif inventory values for that period. During this season, according to the AirParif inventory, the heating sector, commercial and residential, amounts to more than 50% of the emission, so that the total emission is highly sensitive to temperature. Note that AirParif recommends the use of the January inventory for both November and December. As the temperatures are generally milder during October than January, one may expect that the inventory is larger than the true fluxes during October, which is then consistent with the negative correction to the fluxes during that period.

Figure 12 shows the 30-day flux estimates, prior and posterior, for each one of the 6-hour periods. As for the results shown in section 4, the inversion has little impact on the fluxes for

the 0-6h and 18-24h periods. On the other hand, the impact is strong for the 6-12h and 12-18h periods. Although the inversion based on the gradients uses less independent observation than the full inversion does, because of fewer sites and of an additional data selection based on the wind direction, the impact of this setup on the flux estimates is larger. One reason is that we have assigned lower uncertainty for the gradients than for the mole fractions as discussed in section 3.6. Another reason is that many measurements that are not used here, in particular those at TRN, but also those crosswind the Paris plume in the vicinity of the agglomeration, are little sensitive to the Île-de-France emissions so that they bring little information to the inversion when assimilating absolute mole fractions. Clearly, the setup of the inversion based on the gradient retains the observations that do constrain the Paris agglomeration emissions, and should be recommended for future studies.

6. Discussion and Conclusions

This paper is a first attempt at estimating the Paris area emissions from measurements of atmospheric CO_2 mole fractions and prior flux knowledge. There is obviously room for improvement in several aspects of the inversion system: the number and spatial distribution of the monitoring stations, the atmospheric transport model including the use of an urban scheme, the setting of concentration at the simulation domain boundaries, the definition of the emissions outside Île-de-France, the definition of the control vector, etc. However, first conclusions of broad implications beyond this first attempt can be drawn, that should guide further inverse modelling developments for Paris and other cities.

The analysis of the CO_2 time series shows significant differences between the measured and modelled mole fractions upwind the Paris city. These differences indicate that the simulated mole fraction at the domain boundaries may be off by several ppm. Although the number of cases is limited, it seems that the boundary concentrations are significantly underestimated when the wind is from the North or North-East (Benelux). These uncertainties on the domain boundaries generate large scale errors in the modelled mole fraction and suggest applying the inversion not on the measurements themselves, but rather on upwind-downwind gradients as was done in section 5. Indeed, the measurement-model agreement is much better for the gradients (Figure 10) than it is for the direct values (Figure 8). It confirms that the large-scale pattern of CO_2 mole fraction, which is not related to the Île-de-France fluxes, is not properly modelled. The information provided by our five-site network does not allow optimizing the

structure of the CO_2 boundary conditions, which is directly prescribed by a coarse scale global inversion. Exploiting the distant sites currently operational in Europe would unlikely improve this situation. In this context, the inversion based upon gradients as presented in section 5 appears more reliable than those of section 4 so that this setup should be our baseline for future improvements. However, both measurements and atmospheric transport simulations indicate that the CO_2 mole fraction signal generated by distant sources outside the Chimere model domain has some spatial structures (see e.g. the variability of modelled values in Figure 10). As a consequence, distant sources and sink do impact the inversion, even when using the concentration gradients, although the resulting biases on the retrieved fluxes are very much reduced compare to the inversion setup of section 4.

The primary purpose of the gradient-based inversion method is to focus the inversion on the signature of city scale emissions by removing most of the upwind signal from the measured and modelled mole fraction data. The upwind signal is defined by the mole fractions at the domain boundaries and by fluxes within the domain but outside the city, that are poorly represented by the model input data and that cannot be constrained using the network of available measurement stations. Uncertainties in these remote fluxes generate large-scale errors that strongly impact the inverted fluxes. Through the removal of the remote flux signature in the input data, the inversion gradient method attempts at overcoming this problem. Our approach relies on the assumption that, due to atmospheric diffusion, the signature of remote fluxes upwind the city is sufficiently homogeneous in space, horizontally and vertically, and time over the path through the city from upwind to downwind sites both located within the afternoon PBL. As a consequence, the main part of such a large-scale signal is removed through the differences between two sites. The validity of this hypothesis is confirmed by the much better agreement between measured and modelled mole fractions as shown through the comparison of Figure 8 and Figure 10.

The drawback of using the gradient-based inversion method is a reduction in the number of observations, in particular with the current monitoring network that only samples a fraction of possible wind directions. Nevertheless, although the number of observations is very much reduced, our inversion system based on the gradient reports significant uncertainty reductions. The smaller observation error on the gradients, compared to the absolute mole fractions, allows assigning smaller values in the **R** vector, which leads to a larger constraint by the available observations. It must also be noted that we assumed a 7-day error correlation time

for the anthropogenic emissions, so that our system shows flux uncertainty reductions, even on days with no valid observation as the flux is constrained by observation of the previous or following days.

The setting of temporal error correlation on prior fluxes is therefore essential for the inversion. Although the results in this paper are mostly derived with a 7-day correlation length, this is a somewhat arbitrary choice, and the results are significantly affected when using different values. In particular, a much shorter value (1 day) leads to very large variations in the posterior daily emissions. For such short correlation length, the days with no valid observations show a posterior emission that is close to the prior value whereas the flux change, from prior to posterior, is large for the days with observations. Further work should be devoted to the assignment of objective correlation lengths based on the processes that lead to emission uncertainties. Climatic conditions in general, and more specifically temperature during the cold season, influence the emission with a time scale that is consistent with synoptic events, i.e. close to a week; the impact of specific events such as holidays, commemorations or strikes have a much shorter time scale, while inventory biases linked to e.g. the emission factors have an impact on the fluxes on time scales of months or even larger.

Our analysis also indicates model-measurement discrepancies at the EIF site that are much larger than at other sites. On the one hand, this is somewhat surprising as measurement inlet in altitude should insure a larger spatial representativeness than at the surface sites and less sensitivity to local, poorly represented, emissions. Usually, tall tower-based measurements are preferred to those at the surface for the estimate of biogenic fluxes. On the other hand, EIF is located close to the centre of the Paris city and is therefore affected by stronger local emissions than the other sites used in this paper. City fluxes are highly heterogeneous while the model used in this paper has a 2 km spatial resolution, does not include information on the 3D structure of the urban canopy, and uses limited information on the CO_2 source injection heights. Such model may then be insufficient to properly account for atmospheric processes that link the surface fluxes to the concentrations at the top of the Eiffel tower. Previous results obtained at MeteoFrance by (Lac et al., 2013) using a high (2 km) resolution meteorological model that includes urban parameterizations, and validated against local meteorological measurements, also show high model-data misfits at EIF, similar to those found in the present paper. (McKain et al., 2012) also show a poor skill at representing the mole fraction at urban

sites, so that the information content of the measurements is not applied for an estimate of the absolute emissions, but rather for a on long term relative change. These findings can be related to our difficulties for modelling urban CO_2 at EIF using a 2 km resolution transport model are typical of the current generation of models. The use of urban sites such as EIF for atmospheric inversion will likely necessitate long term research by the inverse modelling and transport modelling communities.

At present, our mesoscale atmospheric transport model cannot reconcile the measurements at the top of the tower with those at the surface in the vicinity of the city, given our set of surface fluxes and inversion settings. Our solution has been to disregard the measurements from the EIF site in a best attempt at inverting the Île-de-France CO_2 fluxes. However, our inability to reproduce the EIF mole fraction measurements cast doubts on the quality of the modelling at the other sites. Indeed, if the atmospheric transport model does not properly simulate the atmospheric vertical transport between the surface and an inlet at 300 m in altitude, it likely misrepresents the link between surface fluxes and atmospheric mole fractions. Conversely, the large modelling errors at EIF may be related to its urban location (and to the strong influence of local urban sources) and this would raise concerns regarding the ability to exploit urban measurements, and therefore to solve for the spatial distribution of the fluxes within the urban area.

The largest differences between the measured and modelled concentrations occur for low wind speeds. For this reason, we have chosen a 2 m s^{-1} wind speed threshold below which the measurements are not used in the inversion. A larger threshold rejects further observations, and reduces the range of inverted daily fluxes. The choice of the threshold is somewhat arbitrary and we have refrained from using a large one to clearly demonstrate the impact of a few situations with low wind-speed. There are several hypotheses for the poor modelling at low wind speed, including larger representativity errors of subgrid patterns, or larger errors in vertical mixing modelling. However, such issues are continuous and there is no indication that the modelling errors disappear between e.g. 2 and 3 m s^{-1}. Thus, further rejection of low wind-speed observations may hide the deficiencies in the atmospheric transport without improving the flux inversion.

We also stress that our analysis is based on measurements during the late fall period. This is a favourable case for the inversion of fossil fuel CO_2 emissions as there is less interference with the biogenic fluxes (Pataki et al., 2007). During spring and summer, the NEE is much larger (in absolute value) and also more uncertain. In fact, during May, the biogenic sink is likely larger than the anthropogenic emissions within Île-de-France as shown by Figure 3 and Figure 4. Individual mole fraction measurements cannot distinguish the origin of the concentration signal while the uncertainties on the biogenic fluxes are larger than those on the anthropogenic fluxes. The gradient inversion method is designed to also minimize this interference of biogenic flux with the constraint on anthropogenic fluxes. Indeed, the theoretical posterior uncertainties indicate little correlations between the retrieved NEE and anthropogenic emissions. However, these results are based on strong assumptions in particular that the spatial and temporal distributions of the NEE fluxes are known within large areas. Therefore, in the real world, the inversion may still attribute some flux changes that are necessary to fit the concentrations to the biogenic rather than anthropogenic fluxes. It is certainly possible to estimate independently the biogenic and fossil fluxes from a large set of measurements but a successful inversion relies on an accurate description of the spatial and temporal distribution of both. A successful anthropogenic emission inversion still requires significant efforts for describing the biogenic fluxes and the use of additional tracers such as ^{14}C to separate the signature of fossil fluxes and biogenic emissions. One future direction is thus to use a more realistic NEE model over the Paris area, that could be calibrated upon local eddy covariance observations (e.g. the method used in (Gerbig et al., 2003)) and satellite land cover and vegetation activity.

The prior estimate of the Île-de-France CO_2 emissions does not account for the human respiration. Yet, within dense urban areas, human respiration can be a significant fraction of the fossil fuel emissions (Ciais et al., 2007) (Widory and Javoy, 2003). Respiration by human beings is a source of CO_2 of typically 1 $kgCO_2\ day^{-1}$ (Prairie and Duarte, 2007) which, assuming a total population of 11.7 millions for the Île-de-France, leads to 4.2 $MtCO_2$ per year, or 8% of the AirParif fossil fuel inventory. Although small, this flux is far from negligible compared to fossil fuel emissions. While the CO_2 mole fraction measurements are sensitive to the human respiration flux, our control vector only accounts for the fossil fuel emissions and NEE fluxes. Although it does not have point sources, the spatial distribution of

the human respiration is broadly similar to that of the fossil fuel emissions, so that the inversion will attribute the human respiration mole fraction signal to the fossil fuel rather than the NEE fluxes. We therefore expect an overestimate of the fossil fuel emission by typically 8% in our inversion that neglects human respiration. A larger percentage may be expected in summer and a smaller in winter due to the seasonal cycle of the fossil fuel emissions that has a larger relative amplitude than that of the human respiration. Improvement of our inversion system should explicitly account for the human respiration, based on the spatial distribution of the population.

One often stated objective of the top-down inversion of fossil fuel CO_2 emissions is to provide an independent verification of the bottom-up estimates, i.e. the inventories (Levin et al., 2011;McKain et al., 2012;Duren and Miller, 2012). However, information about the spatial and temporal distribution of the emissions has to be used for inverse modelling to limit aggregation errors on the overall budget. In our case, the number of monitoring stations is far too small to independently invert the spatial distribution of the emissions. We have been able to rely on the comprehensive distribution from AirParif. With a larger number of monitoring stations, it may be possible to estimate some information about the flux spatial distribution, but atmospheric transport is not a reversible process and some accurate information about the spatial distribution will likely be needed, so that the atmospheric inversion cannot be seen as independent from the inventories, but rather as a mean to verify or refine them. In addition, as long as the accuracy on the atmospheric transport makes does not allow using night-time or morning measurements, it will not be possible to monitor the daily cycle of the emissions. Thus, the computation of daily or monthly fluxes requires some robust information about the daily cycle that should rely on inventories. Thus, again, our top-down emission estimate is far from independent from the bottom-up inventory.

Although the inversion procedure provides a posterior uncertainty estimate, one should interpret this uncertainty with caution. Indeed, the mathematical framework used here relies on a number of hypotheses, some of which are crude approximations of the reality, such as the spatial and temporal correlations in the flux uncertainties or the unbiased atmospheric transport modelling. The impact of these assumptions has not been quantified. Although we have no “truth” to benchmark the inversion results, and there are not even enough

measurement sites to perform 'leave-one-out' tests, one can perform some sanity checks on the results. One sanity check is the comparison of the measured and modelled mole fractions (Figure 8 and Figure 10). The analysis of these figures confirms the ability of our inversion to model the concentration gradients much better than the individual absolute measurements. Nevertheless, we note that the posterior misfit (≈2.5 ppm) is still a significant fraction of the signal that is analysed (10-20 ppm). The crucial question is whether the atmospheric modelling error is random or a bias and we have no element to answer that question. The other sanity check consists in analysing the validity of the retrieved daily fluxes (Figure 11). In this respect, the daily fluxes show day-to-day variations that are suspicious, although not refutable at this stage. A result that points in favour of the flux inversions shown here is the significant reduction from the prior during a period with temperatures above the seasonal normal, and the negative correction of the emissions during November from the prior value that is based on an inventory simulating January emissions. A single such event is certainly not sufficient to validate the inversion system, however. We shall apply the same inversion setup to more than a year of measurements and analyse the results with respect to the temperature anomaly or other short-term event that may have a significant influence on the Île-de-France CO_2 emissions. More measurement sites are needed to better evaluate the skill of the inversion. The deployment of a network of 5 sites around Paris within the framework of the CarboCount-City project will help in this direction. In addition, inlet at different altitudes will be installed on the Eiffel tower station for a better assessment of the CO_2 vertical distribution and transport. These will be most useful for the longer-term objective of improving the atmospheric transport modelling within the city, which may allow the EIF measurements to be used by the inversion system.

Acknowledgments

This study was conducted within the ANR CO2-Megaparis project and was made possible thanks to funding from the CarboCount and CarboCount-city projects that are co-funded by the Climate KIC program of the European Institute of Technology. Gregoire Broquet acknowledges funding and support from the Chaire industrielle BridGES, a joint research program between Thales Alenia Space, Veolia, Université de Versailles Saint Quentin en Yvelines, CEA and CNRS. We thank Lin Wu and Isabelle Pison for assistance as well as all the developers of the AirParif inventory.

References

Boussetta, S., Balsamo, G., Beljaars, A., Panareda, A. A., Calvet, J. C., Jacobs, C., van den Hurk, B., Viterbo, P., Lafont, S., Dutra, E., Jarlan, L., Balzarolo, M., Papale, D., and van der Werf, G.: Natural land carbon dioxide exchanges in the ECMWF integrated forecasting system: Implementation and offline validation, J Geophys Res-Atmos, 118, 5923-5946, Doi 10.1002/Jgrd.50488, 2013.

Broquet, G., Chevallier, F., Rayner, P., Aulagnier, C., Pison, I., Ramonet, M., Schmidt, M., Vermeulen, A. T., and Ciais, P.: A European summertime CO2 biogenic flux inversion at mesoscale from continuous in situ mixing ratio measurements, J Geophys Res-Atmos, 116, Artn D23303, doi 10.1029/2011jd016202, 2011.

Broquet, G., Chevallier, F., Breon, F. M., Kadygrov, N., Alemanno, M., Apadula, F., Hammer, S., Haszpra, L., Meinhardt, F., Morgui, J. A., Necki, J., Piacentino, S., Ramonet, M., Schmidt, M., Thompson, R. L., Vermeulen, A. T., Yver, C., and Ciais, P.: Regional inversion of CO2 ecosystem fluxes from atmospheric measurements: reliability of the uncertainty estimates, Atmos Chem Phys, 13, 9039-9056, Doi 10.5194/Acp-13-9039-2013, 2013.

Chevallier, F., Ciais, P., Conway, T. J., Aalto, T., Anderson, B. E., Bousquet, P., Brunke, E. G., Ciattaglia, L., Esaki, Y., Frohlich, M., Gomez, A., Gomez-Pelaez, A. J., Haszpra, L., Krummel, P. B., Langenfelds, R. L., Leuenberger, M., Machida, T., Maignan, F., Matsueda, H., Morgui, J. A., Mukai, H., Nakazawa, T., Peylin, P., Ramonet, M., Rivier, L., Sawa, Y., Schmidt, M., Steele, L. P., Vay, S. A., Vermeulen, A. T., Wofsy, S., and Worthy, D.: CO2 surface fluxes at grid point scale estimated from a global 21 year reanalysis of atmospheric measurements, J Geophys Res-Atmos, 115, Artn D21307, doi 10.1029/2010jd013887, 2010.

Ciais, P., Bousquet, P., Freibauer, A., and Naegler, T.: Horizontal displacement of carbon associated with agriculture and its impacts on atmospheric CO2, Global Biogeochem Cy, 21, Artn Gb2014, doi 10.1029/2006gb002741, 2007.

Desroziers, G., Berre, L., Chapnik, B., and Poli, P.: Diagnosis of observation, background and analysis-error statistics in observation space, Q J Roy Meteor Soc, 131, 3385-3396, Doi 10.1256/Qj.05.108, 2005.

Duren, R. M., and Miller, C. E.: COMMENTARY: Measuring the carbon emissions of megacities, Nat Clim Change, 2, 560-562, 2012.

Gerbig, C., Lin, J. C., Wofsy, S. C., Daube, B. C., Andrews, A. E., Stephens, B. B., Bakwin, P. S., and Grainger, C. A.: Toward constraining regional-scale fluxes of CO2 with atmospheric observations over a continent: 1. Observed spatial variability from airborne platforms, J Geophys Res-Atmos, 108, Artn 4756, doi 10.1029/2002jd003018, 2003.

Gurney, K. R., Law, R. M., Denning, A. S., Rayner, P. J., Baker, D., Bousquet, P., Bruhwiler, L., Chen, Y. H., Ciais, P., Fan, S., Fung, I. Y., Gloor, M., Heimann, M., Higuchi, K., John, J., Maki, T., Maksyutov, S., Masarie, K., Peylin, P., Prather, M., Pak, B. C., Randerson, J., Sarmiento, J., Taguchi, S., Takahashi, T., and Yuen, C. W.: Towards robust regional estimates of CO2 sources and sinks using atmospheric transport models, Nature, 415, 626-630, Doi 10.1038/415626a, 2002.

Gurney, K. R., Razlivanov, I., Song, Y., Zhou, Y. Y., Benes, B., and Abdul-Massih, M.: Quantification of Fossil Fuel CO2 Emissions on the Building/Street Scale for a Large US City, Environ Sci Technol, 46, 12194-12202, Doi 10.1021/Es3011282, 2012.

Kort, E. A., Frankenberg, C., Miller, C. E., and Oda, T.: Space-based observations of megacity carbon dioxide, Geophys Res Lett, 39, Artn L17806, doi 10.1029/2012gl052738, 2012.

Lac, C., Donnelly, R. P., Masson, V., Pal, S., Riette, S., Donier, S., Queguiner, S., Tanguy, G., Ammoura, L., and Xueref-Remy, I.: CO2 dispersion modelling over Paris region within the CO2-MEGAPARIS project, Atmos Chem Phys, 13, 4941-4961, Doi 10.5194/Acp-13-4941-2013, 2013.

Lauvaux, T., Pannekoucke, O., Sarrat, C., Chevallier, F., Ciais, P., Noilhan, J., and Rayner, P. J.: Structure of the transport uncertainty in mesoscale inversions of CO2 sources and sinks using ensemble model simulations, Biogeosciences, 6, 1089-1102, 2009.

Lauvaux, T., Schuh, A. E., Uliasz, M., Richardson, S., Miles, N., Andrews, A. E., Sweeney, C., Diaz, L. I., Martins, D., Shepson, P. B., and Davis, K. J.: Constraining the CO2 budget of the corn belt: exploring uncertainties from the assumptions in a mesoscale inverse system, Atmos Chem Phys, 12, 337-354, Doi 10.5194/Acp-12-337-2012, 2012.

Levin, I., Hammer, S., Eichelmann, E., and Vogel, F. R.: Verification of greenhouse gas emission reductions: the prospect of atmospheric monitoring in polluted areas, Philosophical transactions. Series A, Mathematical, physical, and engineering sciences, 369, 1906-1924, 10.1098/rsta.2010.0249, 2011.

Lopez, M., Schmidt, M., Delmotte, M., Colomb, A., Gros, V., Janssen, C., Lehman, S. J., Mondelain, D., Perrussel, O., Ramonet, M., Xueref-Remy, I., and Bousquet, P.: CO, NOx and (CO2)-C-13 as tracers for fossil fuel CO2: results from a pilot study in Paris during winter 2010, Atmos Chem Phys, 13, 7343-7358, Doi 10.5194/Acp-13-7343-2013, 2013.

McKain, K., Wofsy, S. C., Nehrkorn, T., Eluszkiewicz, J., Ehleringer, J. R., and Stephens, B. B.: Assessment of ground-based atmospheric observations for verification of greenhouse gas emissions from an urban region, P Natl Acad Sci USA, 109, 8423-8428, Doi 10.1073/Pnas.1116645109, 2012.

Menut, L., Bessagnet, B., Khvorostyanov, D., Beekmann, M., Blond, N., Colette, A., Coll, I., Curci, G., Foret, G., Hodzic, A., Mailler, S., Meleux, F., Monge, J. L., Pison, I., Siour, G., Turquety, S., Valari, M., Vautard, R., and Vivanco, M. G.: CHIMERE 2013: a model for regional atmospheric composition modelling, Geosci Model Dev, 6, 981-1028, Doi 10.5194/Gmd-6-981-2013, 2013.

Nehrkorn, T., Henderson, J., Leidner, M., Mountain, M., Eluszkiewicz, J., McKain, K., and Wofsy, S.: WRF Simulations of the Urban Circulation in the Salt Lake City Area for CO2 Modeling, J Appl Meteorol Clim, 52, 323-340, Doi 10.1175/Jamc-D-12-061.1, 2013.

Nordbo, A., Jarvi, L., Haapanala, S., Wood, C. R., and Vesala, T.: Fraction of natural area as main predictor of net CO2 emissions from cities, Geophys Res Lett, 39, Artn L20802, doi 10.1029/2012gl053087, 2012.

Pal, S., Xueref-Remy, I., Ammoura, L., Chazette, P., Gibert, F., Royer, P., Dieudonne, E., Dupont, J. C., Haeffelin, M., Lac, C., Lopez, M., Morille, Y., and Ravetta, F.: Spatio-temporal variability of the atmospheric boundary layer depth over the Paris agglomeration: An assessment of the impact of the urban heat island intensity, Atmos Environ, 63, 261-275, Doi 10.1016/J.Atmosenv.2012.09.046, 2012.

Pataki, D. E., Alig, R. J., Fung, A. S., Golubiewski, N. E., Kennedy, C. A., McPherson, E. G., Nowak, D. J., Pouyat, R. V., and Lankao, P. R.: Urban ecosystems and the North American carbon cycle, Global Change Biol, 12, 2092-2102, Doi 10.1111/J.1365-2486.2006.01242.X, 2006.

Pataki, D. E., Xu, T., Luo, Y. Q., and Ehleringer, J. R.: Inferring biogenic and anthropogenic carbon dioxide sources across an urban to rural gradient, Oecologia, 152, 307-322, Doi 10.1007/S00442-006-0656-0, 2007.

Peylin, P., Rayner, P. J., Bousquet, P., Carouge, C., Hourdin, F., Heinrich, P., Ciais, P., and Contributors, A.: Daily CO2 flux estimates over Europe from continuous atmospheric measurements: 1, inverse methodology, Atmos Chem Phys, 5, 3173-3186, 2005.

Prairie, Y. T., and Duarte, C. M.: Direct and indirect metabolic CO2 release by humanity, Biogeosciences, 4, 215-217, 2007.

Shepson, P. B., Cambaliza, M., Davis, K., Gurney, K., Lauvaux, T., Richardson, N., Richardson, S., Sweeney, C., and Turnbull, J.: Indianapolis flux experiment (INFLUX): Experiment design and new results regarding measurements of urban-area CO2 and CH4 emission fluxes, Abstr Pap Am Chem S, 242, 2011.

Tarantola, A.: Inverse problem theory and methods for model parameter estimation, Society for Industrial and Applied Mathematics, Philadelphia, PA, xii, 342 p. pp., 2005.

Widory, D., and Javoy, M.: The carbon isotope composition of atmospheric CO2 in Paris, Earth Planet Sc Lett, 215, 289-298, Doi 10.1016/S0012-821x(03)00397-2, 2003.

Zhao, C. L., and Tans, P. P.: Estimating uncertainty of the WMO mole fraction scale for carbon dioxide in air, J Geophys Res-Atmos, 111, Artn D08s09, doi 10.1029/2005jd006003, 2006.

Tables and captions

Table 1 : Information about the CO_2 measuring stations that are used in this paper.

Location	Acronym	Latitude [°]	Longitude [°]	Height AGL [m]	Distance from Paris centre [km]
Eiffel Tower	EIF	48.8582	2.2946	300	4 (W)
Montgé-en-Goële	MON	49.0284	2.7489	9	35 (NE)
Gonesse	GON	48.9908	2.4446	4	16 (N)
Gif sur Yvette	GIF	48.7100	2.1475	7	23 (SW)
Trainou Forest	TRN	47.9647	2.1125	180	101 (S)

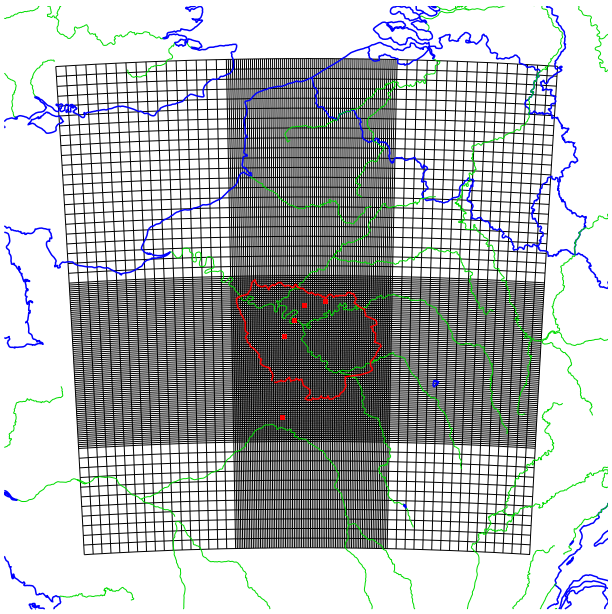

Figure 1 : Map of the study area showing the location of the continuous CO_2 measurement stations that are used in this paper (red dots). The black lines show the model grid with a 2 km resolution at the centre, and 10 km on the sides. The red line shows the limits of the Île-de-France region.

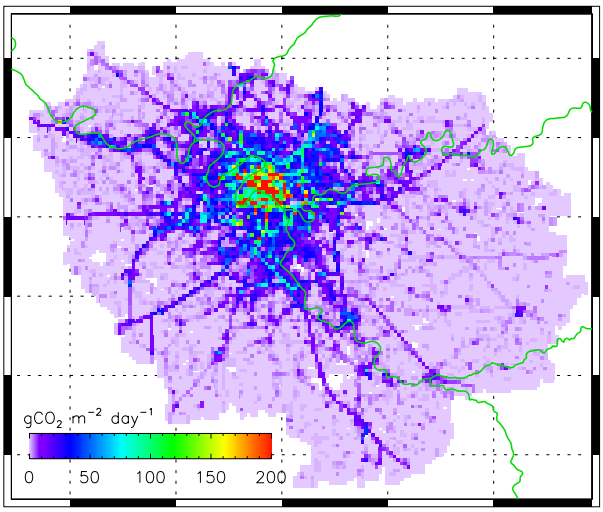

Figure 2 : Typical day-total CO_2 emissions of Île-de-France, according to AirParif year 2008 inventory, for a weekday in October. The point sources are not included in this map. The emissions are provided for the area outlined in red in Figure 1. The resolution is 1 km. The grid is 0.2° in latitude and 0.4° in longitude.

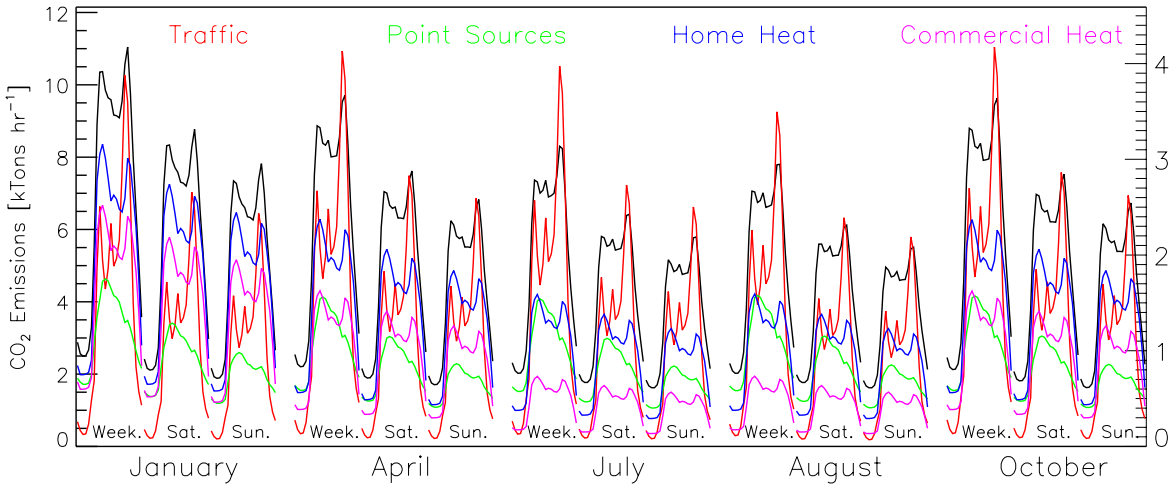

Figure 3: Temporal variation of the main CO_2 emission sectors according to the AirParif inventory for the whole Ile de France region. The figure shows, for 5 typical months and 3 typical days (Weekday, Satuday, Sunday), the hourly CO_2 emissions. The black line is the total emission (left scale) while the four coloured lines are for different sectors (right scale).

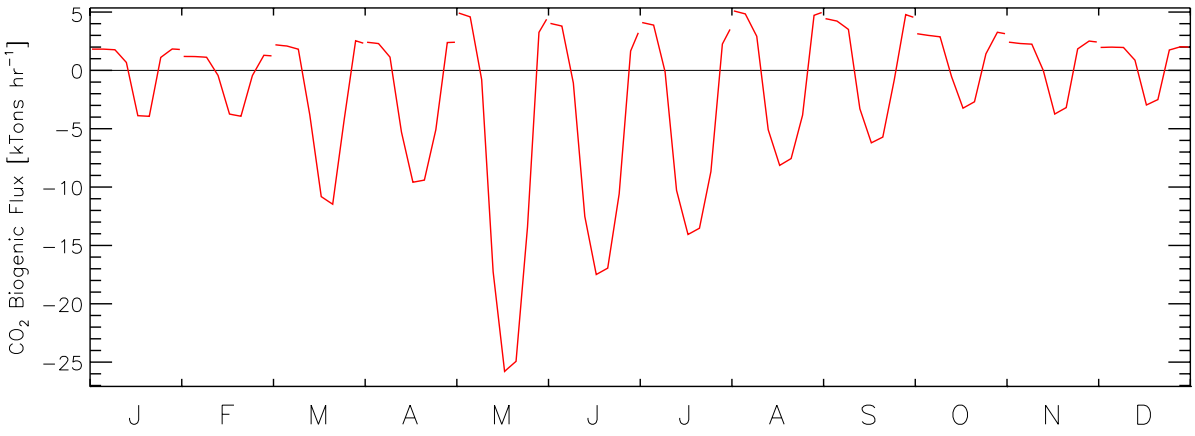

Figure 4: Mean diurnal cycle of the biogenic flux (Net Ecosystem exchange) for the 12 calendar months and for the same area as in Figures 2 and 3 which is outlined in red in Figure 1. The values were derived from an average of the C-Tessel simulations.

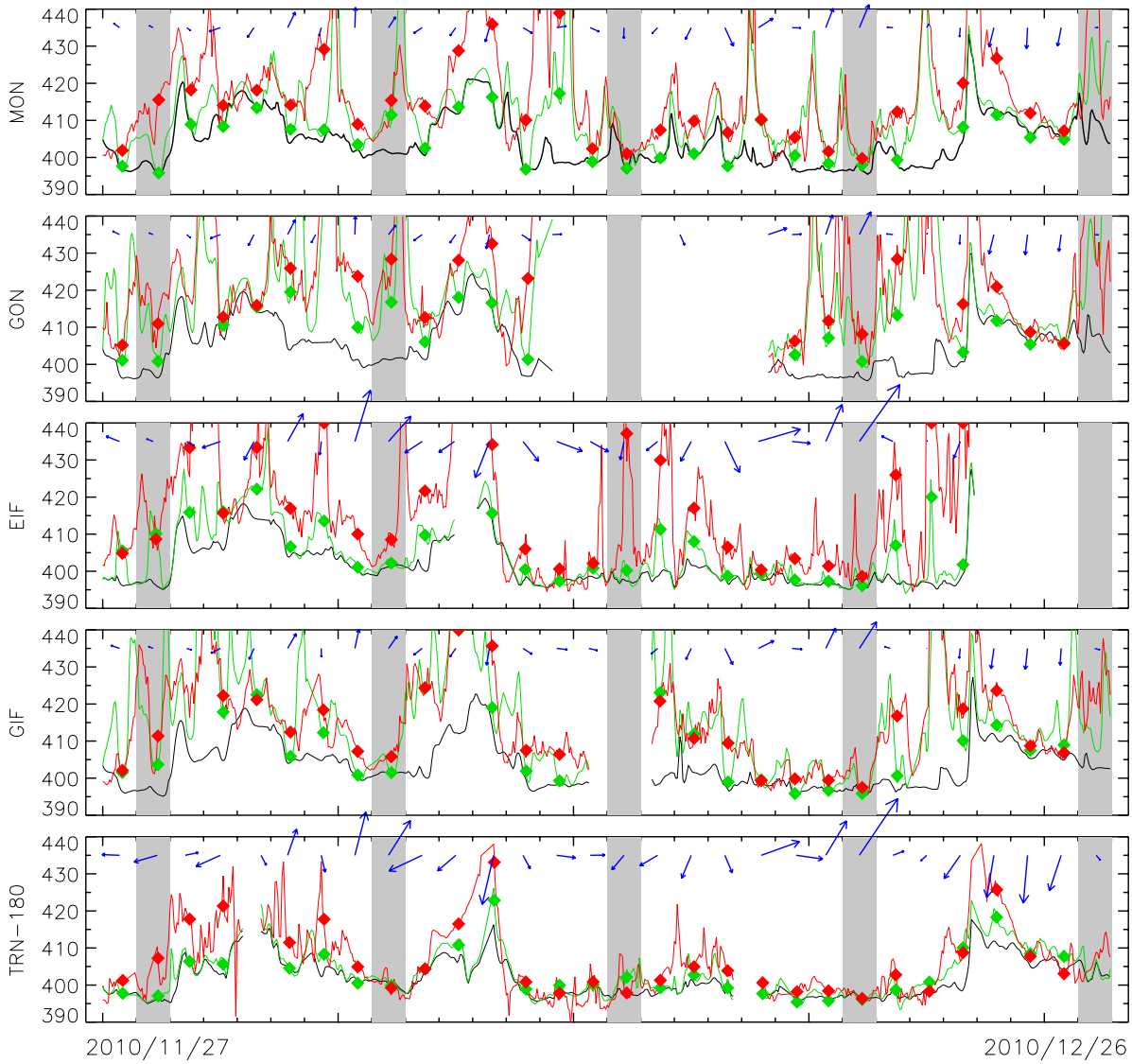

Figure 5: Time series of the measured (red) and modelled (green) CO_2 mole fraction [ppm] for the five sites used in this paper (See Table 1). The black line is the modelled mole fraction that is transported from the domain boundaries, with additional contribution from anthropogenic emissions outside the Île-de-France region (Edgar fluxes). The green line shows the modelled mole fraction that includes the same contributions, plus the biogenic fluxes within the modelling domain and the anthropogenic emissions within the Île-de-France region. Red are the observations. Note that there are some time periods when no measurements are available due to either calibration processes or, more rarely, failure of the monitoring instrumentation. For such periods, modelling results are not shown. The symbols show the mean of the afternoon measurement/model values that are used for the inversion. The blue arrows indicate the wind speed and direction at noon. A length equivalent to 1 day

on the X-axis is for a wind speed of 10 m/s. This figure is for the 30 days period starting on 2010/11/27. Grey shaded areas indicate Sundays.

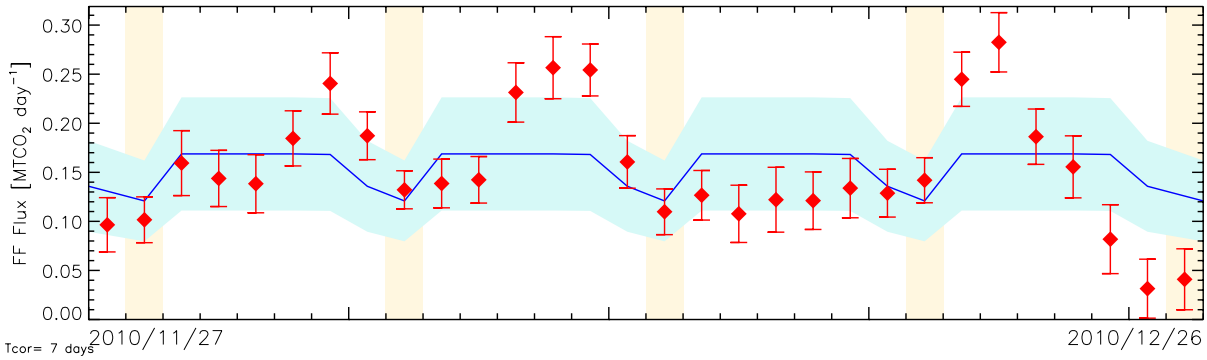

Figure 6 : Daily flux estimates of the anthropogenic emission for the 30 days of the period. The blue line and shading shows the prior flux according to the AirParif inventory together with its assumed uncertainty. Yellow shading indicate Sundays; note the weekly cycle with lower values during Saturdays and Sundays. The red symbols and bars show the posterior estimates with their uncertainty range. This figure is for the Nov-Dec period. A similar figure for the Oct-Nov period is shown in the supplementary material.

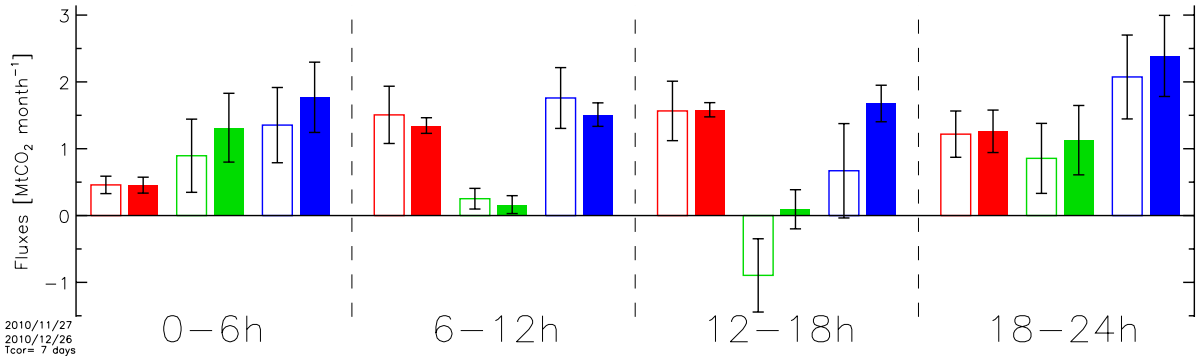

Figure 7 : Total flux estimates over the full 30 day period, for the 4 6-hour periods. Red is for the anthropogenic emissions, green is for the biogenic fluxes while blue is for the total. The prior estimates are shown as open rectangles while the posterior are shown as filled rectangles. This figure is for the Nov-Dec period. A similar figure for the Oct-Nov period is shown in the supplementary material.

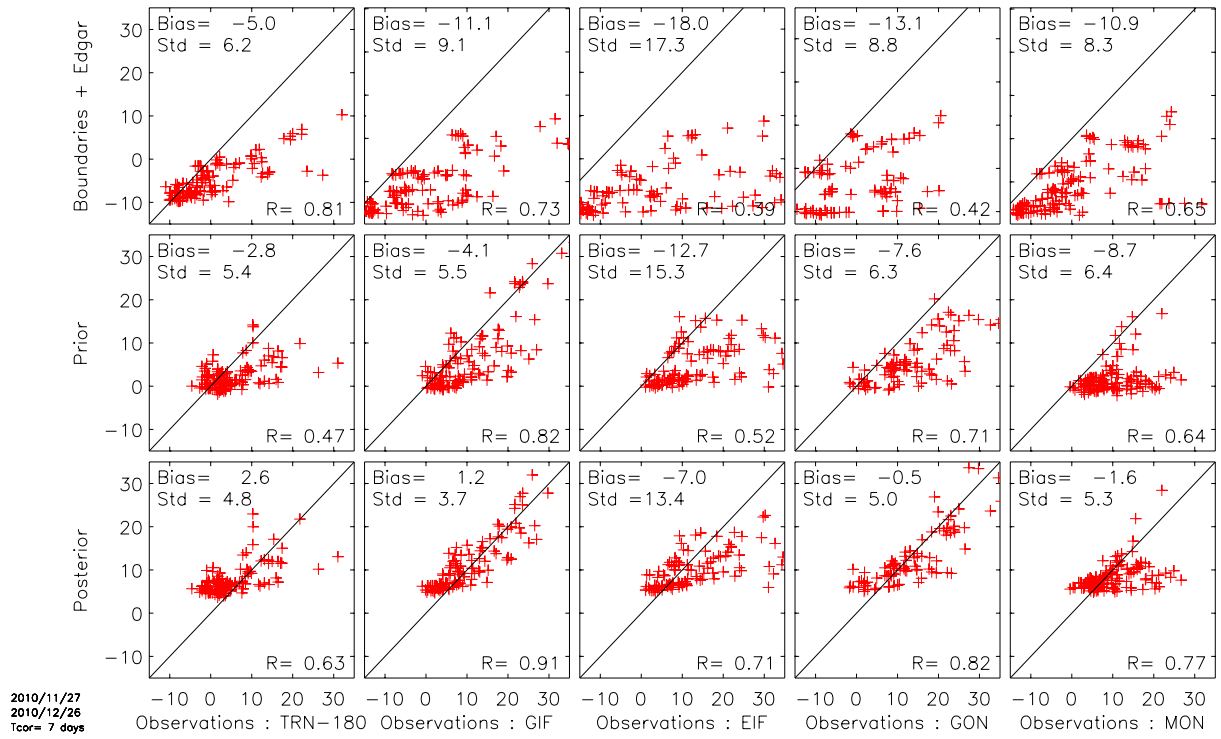

Figure 8 : Scatter plot of the measured and modelled concentration for the 5 stations used in this paper. The first row shows the mole fraction simulated using the boundary conditions and the anthropogenic emissions outside Île-de-France (y_F in equation 1) against the measurements. The values are offset by the mean of the measured concentrations. The second row shows the concentration estimates derived from the prior values for the biogenic fluxes and anthropogenic fluxes against the corrected measurements (i.e. y - yF in equation 1). The last row is the same but using the posterior estimates. This figure is for the Nov-Dec period. A similar figure for the Oct-Nov period is shown in the supplementary material.

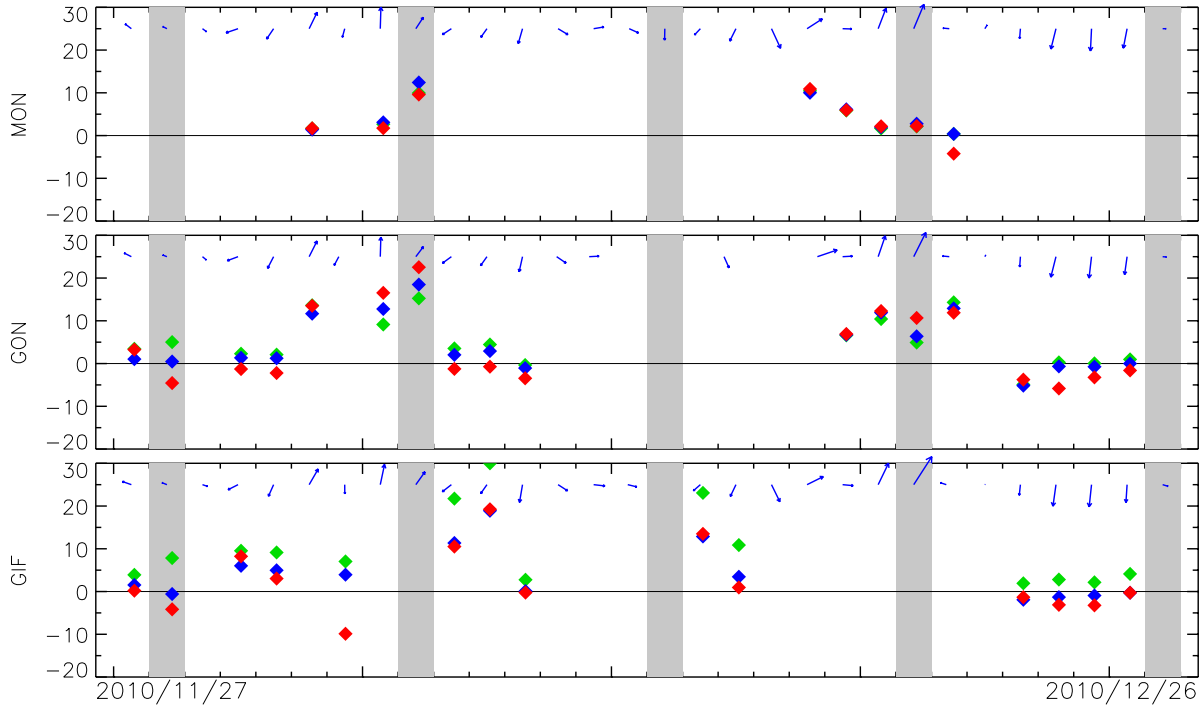

Figure 9 : Time series of the mole fraction differences between a station (Y-axis label) and another one used as a reference (either GIF or GON) and selected based on the wind direction (see section 3.3). The symbols show the mean afternoon concentrations (12AM-4PM) for the measurements (red), the prior (green) and the posterior (blue) estimates. As in Figure 5, the arrows indicate the wind speed and direction. A similar figure for the other time period is shown in the supplementary material.

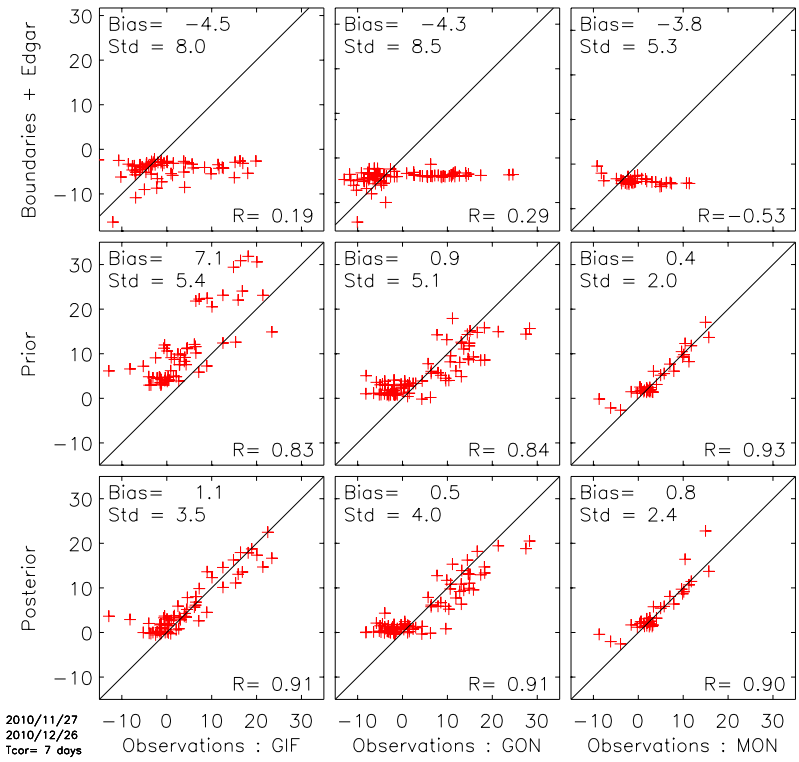

Figure 10: Same as Figure 8 but for the mole fraction gradients where the reference measurements is selected according to the wind direction. The TRN and EIF stations are not used. A similar figure for the other time period is shown in the supplementary material.

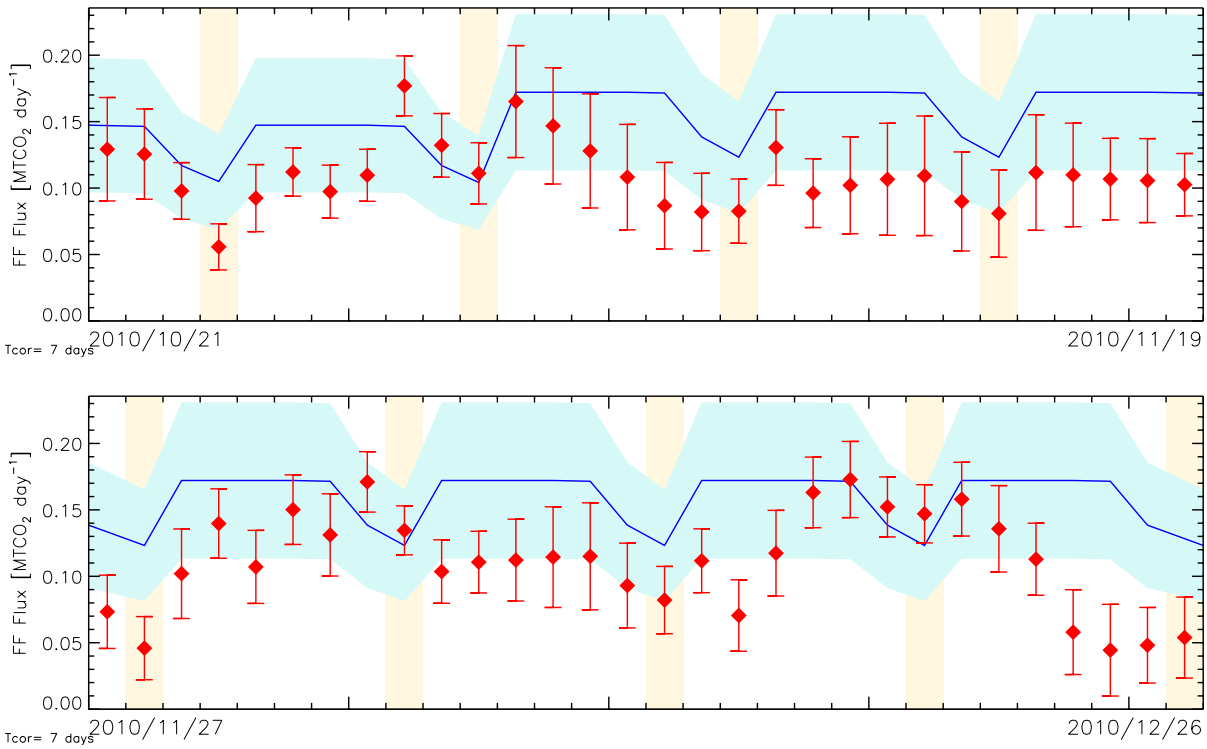

Figure 11 : Same as Figure 6 but for the inversion based on the concentration gradients, and using only the three measuring stations in the vicinity of the Paris city. Both 30-day periods are shown.

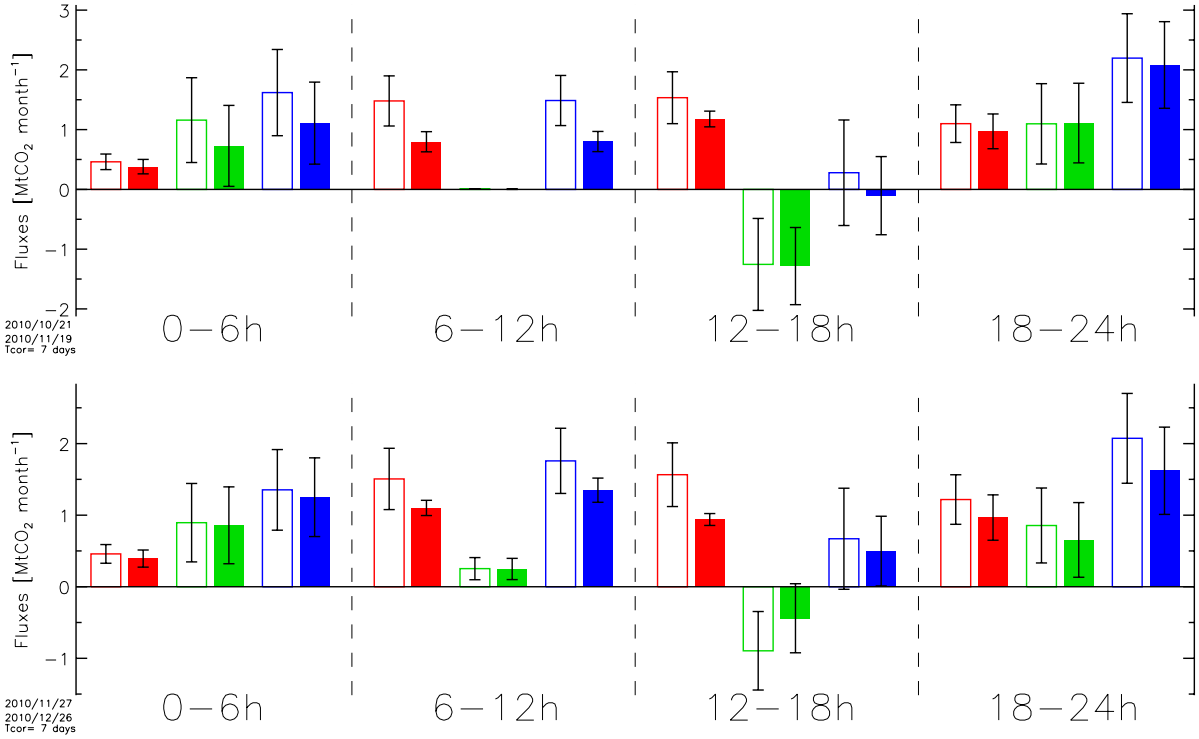

Figure 12 : Same as Figure 7 but for the inversion based on the mole fraction gradients, and using only the three measuring stations in the vicinity of the Paris city. Both 30-day periods are shown.

Supplementary material

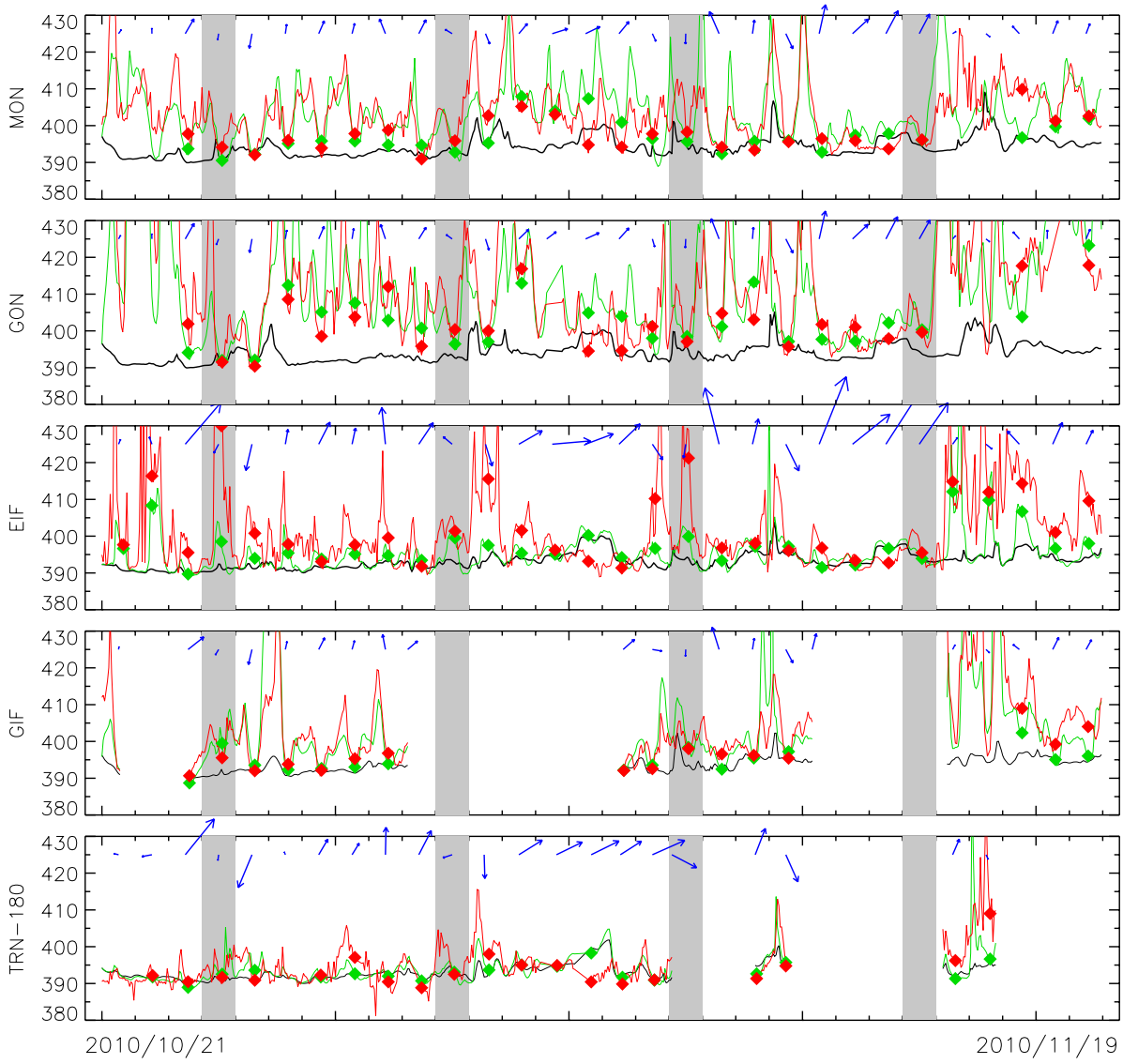

Figure S- 1: Same as Figure 5 but for the 30 days period starting on October 21st.

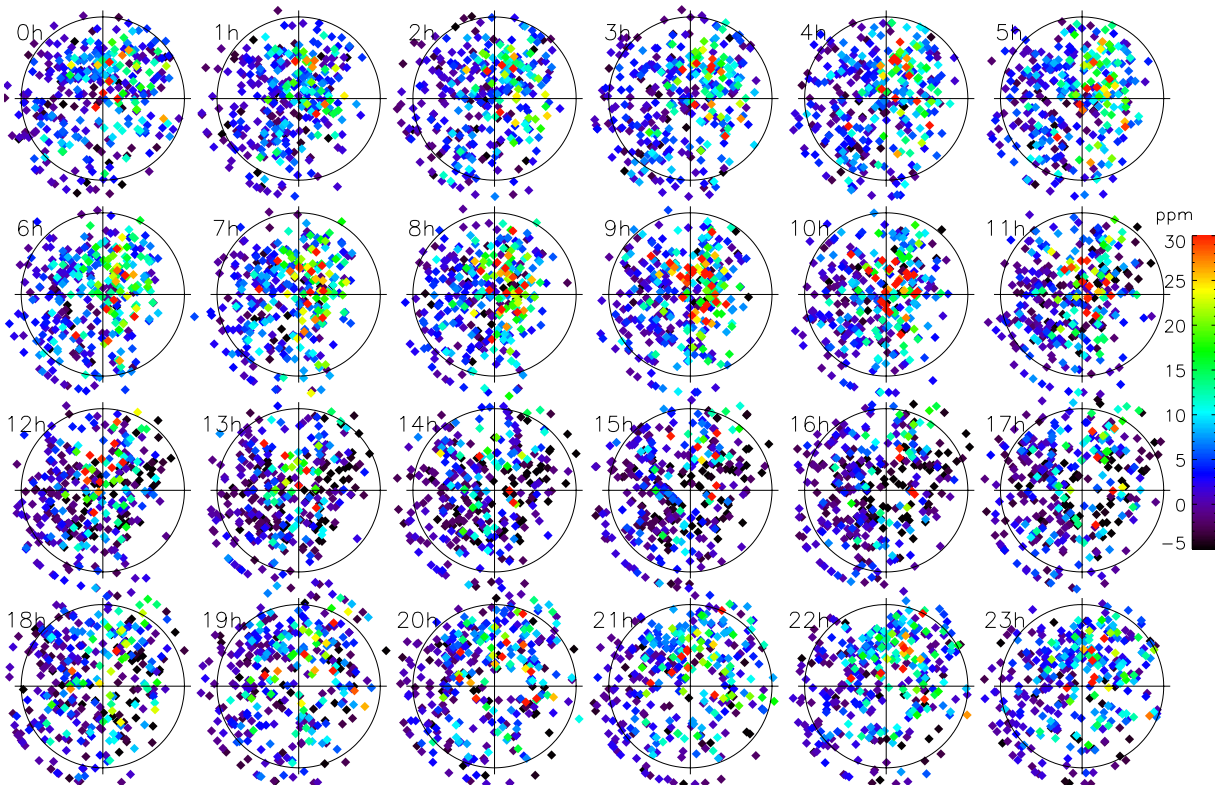

Figure S- 2 : Measurement-Model difference in CO_2 mole fraction at the EIF site as a function of time, wind speed and direction. The position of the symbols indicates the wind direction (top-right is for a wind from the North-East) and speed (the circles indicate a wind of 10 m s^{-1}). The wind speeds have been bounded at 12 m s^{-1}.

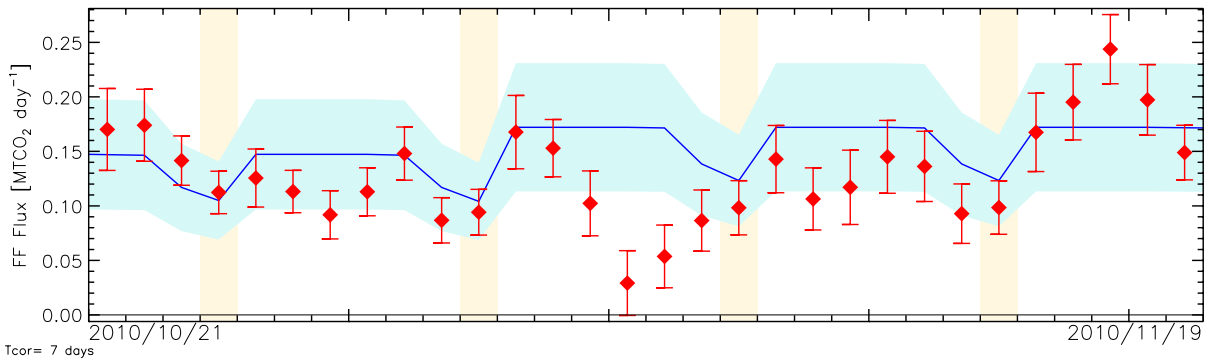

Figure S- 3 : Same as Figure 6 but for the 30 days period starting on October 21st.

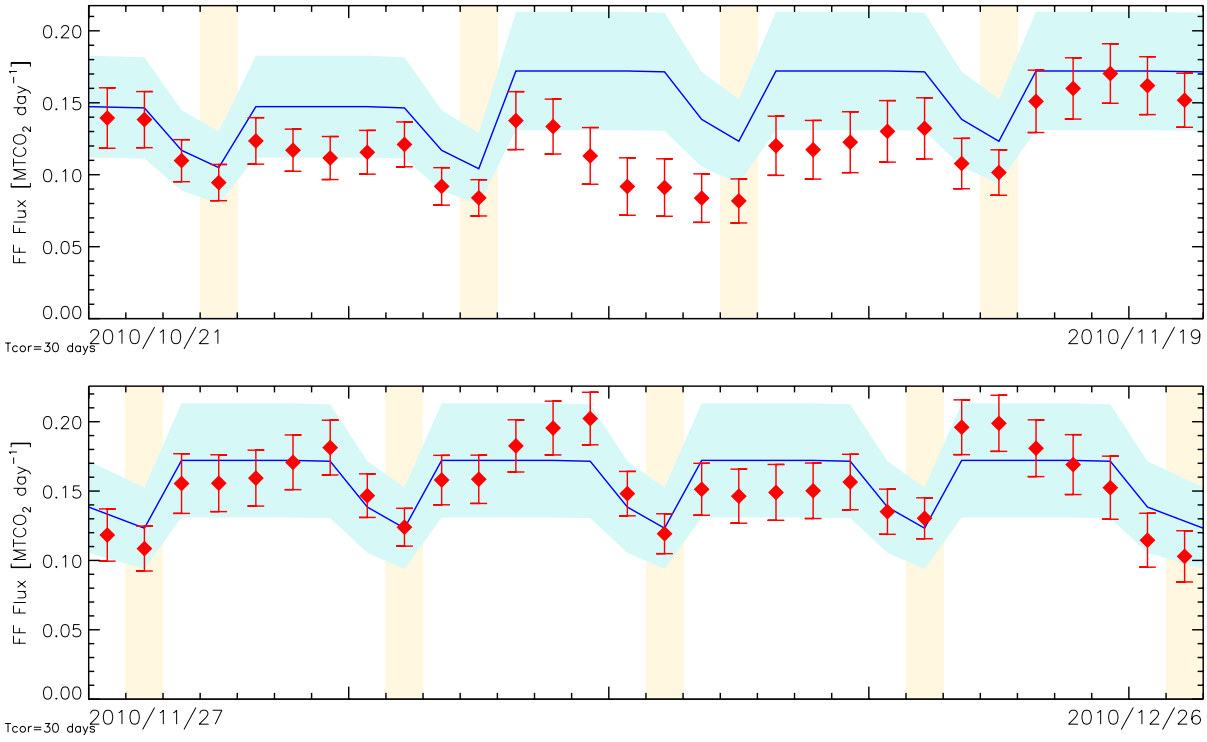

Figure S- 4: Same as Figure 6 but the covariance matrix ***B*** is build assuming a 30 days correlation time.

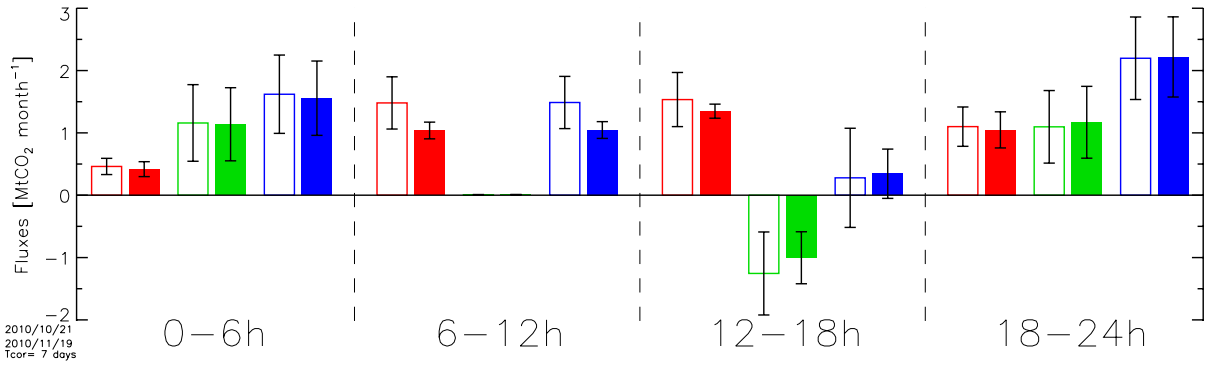

Figure S- 5 : Same as Figure 7 but for the 30-day period starting on October 21st.

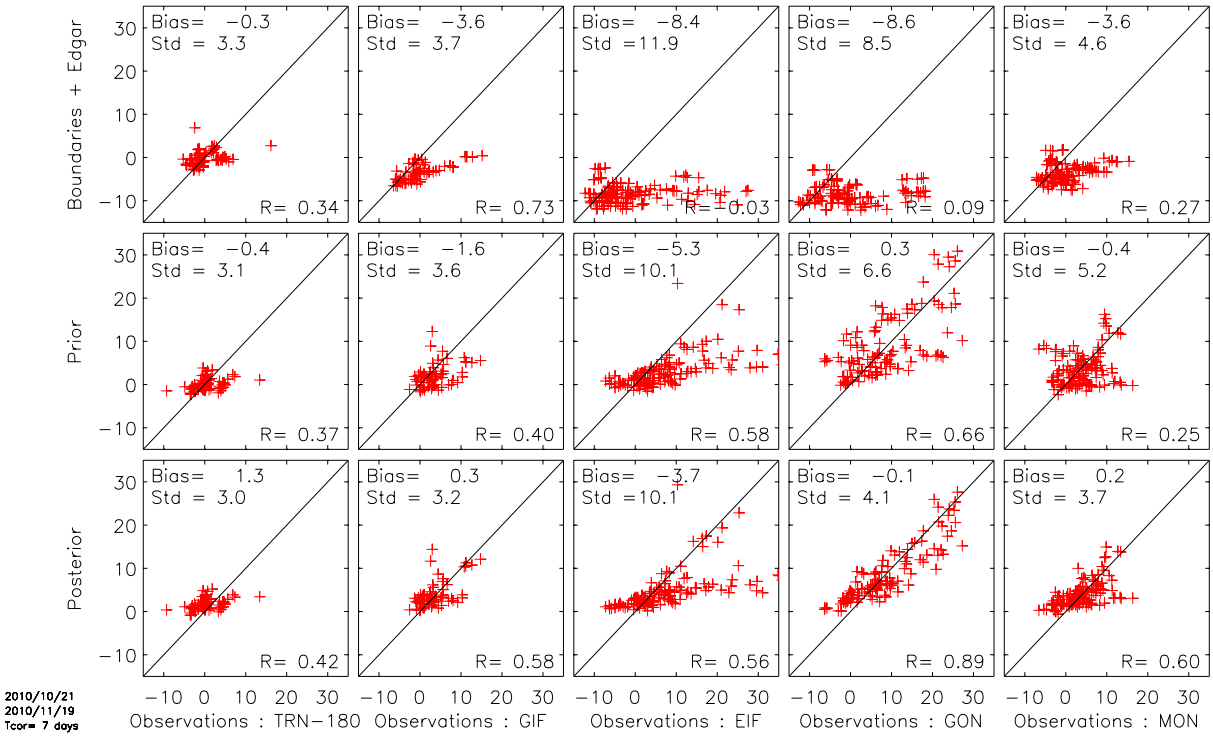

Figure S- 6: Same as Figure 8 but the 30-day period starting on October 21st.

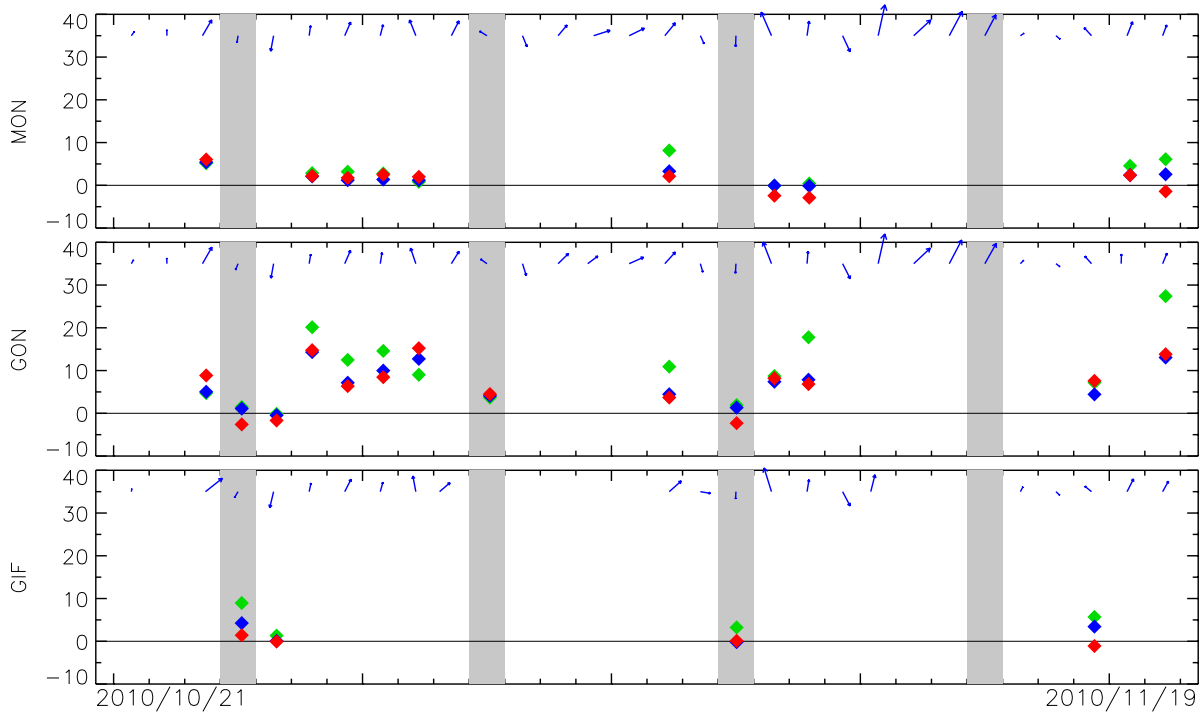

Figure S- 7 : Same as Figure 9 but for the 30-day period starting on October 21st.

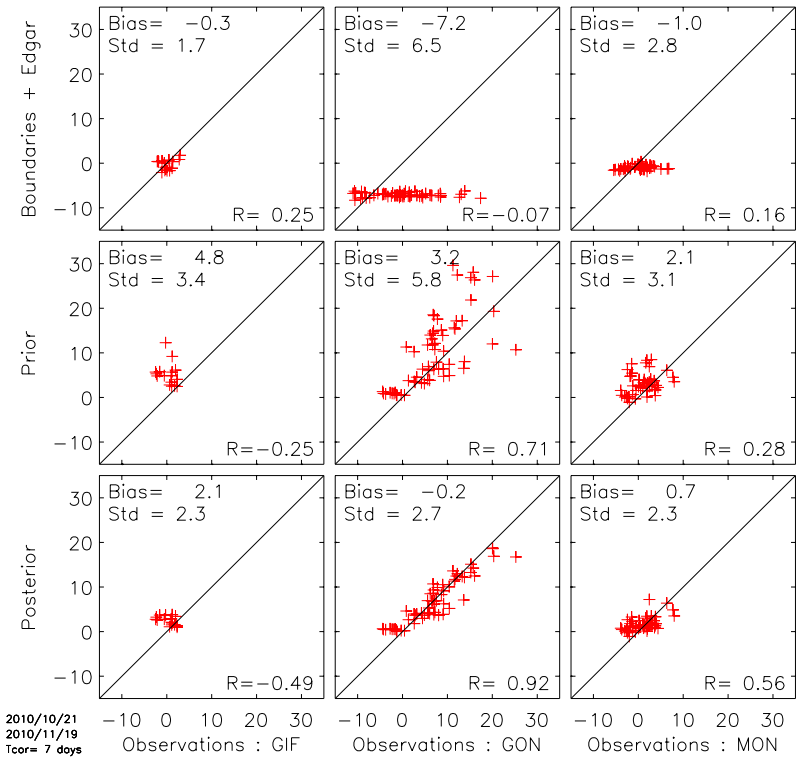

Figure S- 8: Same as Figure 10 but for the 30-day period starting on October 21st.